Astron. Astrophys. 331, 291–313 (1998)

ASTRONOMY
AND
ASTROPHYSICS

A comet dust model for the β Pictoris disk

Aigen Li and J. Mayo Greenberg

Laboratory Astrophysics, University of Leiden, Postbus 9504, 2300 RA Leiden, The Netherlands
(e-mail: agli@strw.LeidenUniv.nl; mayo@rulhl1.LeidenUniv.nl)

Received 26 June 1997 / Accepted 19 September 1997

Abstract. The 10 μm silicate emission feature and the continuum emission from near infrared to millimeter of the dust in the disk of β Pictoris may be derived by assuming that the dust is continually replenished by comets orbiting close to the star. The basic, initial dust shed by the comets is taken to be the fluffy aggregates of interstellar silicate core-organic refractory mantle dust grains (with an additional ice mantle in the outer region of the disk). The heating of the dust is primarily provided by the organic refractory mantle absorption of the stellar radiation. The temperature of some of the particles close to the star is sufficient to crystallize the initially amorphous silicates. The dust grains are then distributed throughout the disk by radiation pressure. The steady state dust distribution of the disk then consists of a mixture of crystalline silicate aggregates and aggregates of amorphous silicate core-organic refractory mantle particles (without/with ice mantles) with variable ratios of organic refractory to silicate mass. The whole disk which extends inward to $\sim$ 1 AU and outward to $\sim$ 2200 AU is divided into three components which are primarily responsible respectively, for the silicate emission, the mid-infrared emission and the far infrared/millimeter emission. As a starting point, the grain size distribution is assumed to be like that observed for comet Halley dust while in the inner regions the distribution of small particles is relatively enhanced which may be attributed to the evaporation and/or fragmentation of large fluffy particles. The dust grains which best reproduce the observations are highly porous, with a porosity around 0.95 or as high as 0.975. The temperature distribution of a radial distribution of such particles provides an excellent match to the silicate 10 μm (plus 11.2 μm) spectral emission as well as the excess continuum flux from the disk over a wide range of wavelengths. These models result in a total mass of dust in the whole disk $\sim 2 \times 10^{27}$ g of which only 10^{-5} – 10^{-4} is hot enough to give the silicate excess emission. The specific mineralogy of crystalline silicates has been discussed.

Key words: stars: individual: β Pictoris – stars: circumstellar matter – stars: planetary systems – ISM: dust – comets: general

Send offprint requests to: J.M. Greenberg

1. Introduction

Since the Infrared Astronomical Satellite (IRAS) detected the so-called "Vega Phenomenon"; i.e., that main sequence stars exhibit large infrared (IR) excesses over the black body emission of their photospheres (Aumann et al. 1984), it has become well established that the "Vega Phenomenon" is not exceptional but rather quite common among the main sequence stars (see Backman & Paresce 1993). Because some detailed questions remain as to how common it is and whether it depends on the fundamental properties of the stars themselves (mass, age, rotation etc.) it constitutes one of the tasks of the ISO photometric infrared survey (cf. Habing et al. 1996). It is generally believed that these IR excesses may be attributed to the thermal emission of circumstellar dust orbiting the central stars which is heated to about 100 K. Among Vega-type stars, β Pictoris (an A5 star, HD 39060, HR 2020) is the most extensively studied one, not only because it has the largest IR excess, but also because its resolved nearly edge-on protoplanetary disk structure (Smith & Terrile 1984; Lagage & Pantin 1994) shows evidence of planet formation and provides clues for us to understand the formation process of our solar system. The observations of the β Pictoris disk cover a wide range of wavelengths from ultraviolet to millimeter: high resolution UV and visual spectral line monitoring by a French group (e.g., Vidal-Madjar et al. 1994 and references therein); optical images of the scattered light (e.g., Paresce & Burrows 1987; Golimowski et al. 1993; Lecavelier des Etangs et al. 1993; etc); infrared and submillimeter photometric measurements (e.g., Telesco et al. 1988; Chini et al. 1991; Zuckerman & Becklin 1993; Harvey et al. 1996; Dominik et al. 1997); and imaging in the infrared (Lagage & Pantin 1994). Special attention has been paid to spectroscopic observations in the near infrared (NIR) region. The first successful discovery of the silicate feature by Telesco & Knacke (1991) and the subsequent confirmations by Aitken et al. (1993) and by Knacke et al. (1993), in particular, the identification of the 11.2 μm feature characteristic of crystalline silicate (Knacke et al. 1993), provided valuable information to help understand better the dust in the disk. In addition to these observational studies, many theoretical investigations have also been performed (e.g., Artymowicz et al. 1989; Backman et al. 1992; Roques et al. 1994; Greenberg

& Li 1996; etc) to infer the properties of the dusty disk: grain sizes, chemical compositions, disk structure and evolution.

In spite of so many observational and theoretical efforts having been devoted to understand β Pictoris, the basic properties of the dust grains in the disk have remained uncertain. The conclusions drawn from some of these earlier works have been either incomplete, inconclusive, or even controversial. With the exception of Greenberg & Li (1996) and Pantin et al. (1997), all models used compact particles. For example, the thermal modeling by Backman et al. (1992) required all particles to be as small as 1 μm, whereas, much larger particles are required to explain the optical light scattering data (Paresce & Burrows 1987). Modeling both the scattered starlight and the far infrared (FIR) emission (Artymowicz et al. 1989) indicated that the particles were approximately between 1 μm and 20 μm. However, in order to fit the millimeter observation, Chini et al. (1991) argued that the typical size of dust grain radii had to be greater than 10 μm and up to at least 1 mm. Telesco & Knacke (1991) pointed out that the particles must be less than 10 μm to give the silicate emission. Aitken et al. (1993) reported that 2 μm grains could reproduce their own observations of the silicate emission feature, using the optical constants of "astronomical silicates" (Draine & Lee 1984). On the other hand, the detailed modeling of Knacke et al. (1993) showed that compact Draine & Lee silicate particles failed to reproduce the silicate feature. This led them to suggest that "the silicate mineral composition is different from that incorporated in the Draine & Lee constants". Their attempts to improve the fits by other silicate mineral compositions were also unsuccessful. The predicted albedo was also different from one model to another (e.g., Artymowicz et al. 1989; Backman et al. 1992). The resultant distributions of dust in the disk (disk structure) were also different. In modeling the spectral energy distribution including millimeter data, Chini et al. (1991) required that the dust particles in the inner $\leq$ 36 AU of the disk were greatly depleted, while Artymowicz et al. (1989) suggested that the inner clearing zone is about $\sim 5 - 15$ AU, and Backman et al. (1992) claimed that the dusty disk extends inward to 1 AU. As far as the dust morphology is concerned, all the models discussed above were based on compact spherical particles. Actually, the aggregation of primary interstellar dust particles in the first stage of star formation should lead to fluffy structure (Krügel & Siebenmorgen 1994; Henning & Stognienko 1996 and references therein) so that the introduction of porous cometary dust grains by Greenberg & Li (1996) was a more logical choice.

The inconsistencies and controversies should not have been a surprise at all, since each of the previous models focused only on the dust grains in a certain region of the disk rather than considering the full disk.The comprehensive modeling of scattered light in the optical band by Artymowicz et al. (1989) placed detailed constraints on the scattering properties of the dust grains and on the dust density distribution in the outer region of the disk ($\geq$ 100 AU), while the dust properties in the inner disk were less or poorly constrained. The dust particles considered by Backman et al. (1992) and Chini et al. (1991) were designed to be responsible for the dust continuum emission, while the now well established silicate spectra were not taken into account (actually, the detection of the detailed silicate structure came later). In modeling the spectral energy distribution, they arbitrarily assumed a power law approximation for the grain absorptivity (emissivity). However, even if the actual wavelength dependent optical constants of dust particles were incorporated in their models, there is no reason to expect the presence of any silicate feature because the dust particles are either too cold or too large to show any excess emission in the silicate wavelength range. Our calculations show that, in the model of Backman et al. (1992), the particles with a typical size (1 μm) in the inner boundary (4.5 AU) are at $\sim$ 250 K; in the model of Chini et al. (1991), the smallest particles (10 μm) in the innermost region of the disk (36 AU) are at about 70 K. Obviously the hottest particles in these models are too cold to provide the silicate emission which is mostly given by particles at $\sim$ 300 K. Contrary to the continuum modeling of Backman et al. (1992) and of Chini et al. (1991), Knacke et al. (1993) and Aitken et al. (1993) only considered the hot particles in the inner disk which are responsible for the silicate emission. It is seen that, in order to obtain a complete picture of the β Pictoris disk, one needs to consider *all* the dust particles distributed in the *entire* disk; namely, both the hot particles which produce the silicate feature and the cold particles which are responsible for the FIR and millimeter emission. It is the aim of this work to model simultaneously both the continuum from the NIR to the millimeter and the silicate feature with a full description of the dust properties over the entire disk.

Considerable evidence exists which shows that the dust particles in the β Pictoris disk cannot be the reservoir left over after star formation. Dynamical studies indicate that the grain destruction time scales due to grain-grain collisions, Poynting-Robertson drag and radiation pressure are shorter than the lifetime of β Pictoris (Backman & Paresce 1993). This indicates that there must be some dust source which continually replenishes the lost particles. Such a source was first suggested as due to comet-like bodies by Weissman (1984). The fact that the structured silicate feature (broad amorphous silicate emission at 9.7 μm with a crystalline silicate feature at 11.2 μm superimposed) is similar to that of some comets including the famous comet Halley and the most recent comet Hale-Bopp (Campins & Ryan 1989; Hanner et al. 1994; Hayward & Hanner 1997) indicates the similarity of cometary dust with the β Pictoris dust. Furthermore, the systematic spectroscopic observations of gaseous elements in the visible or in the ultraviolet carried out by the French group showed that the spectral lines CaII, MgII, FeII, AlIII, AlII, CIV, CI and CO show strong time variations and are almost always redshifted relative to the stellar spectra (Vidal-Madjar et al. 1994 and references therein). These variations can be explained to result from the evaporation of the dust grains shed from comet-like bodies falling on the star as a consequence of planet perturbation (Beust et al. 1990). It may be of interest to note that massive bombardment of the planets by cometary bodies lasted more than 500 million years in our early solar system (Chyba et al. 1994) so that the presence of comets in β Pictoris, which is much younger than this (Paresce

1991; Crifo et al. 1997) is not exceptional. Thus we assume that the dust particles in the β Pictoris disk are of cometary origin; i.e., fluffy aggregates of primitive interstellar grains.

In this work, we simultaneously model both the silicate spectra and the continuum from NIR to millimeter. The scattered light in the optical band undoubtedly provides useful constraints on the dust properties. Due to the complexity of obtaining a precise solution of the porous particles scattering problem, we have not modeled the scattered light in this work. Sect. 2 discusses the dust compositions, sizes, and spatial density distribution. The modeling methods are described in Sect. 3. Sect. 4 presents the model results which provide the best fit to the observations. In Sect. 5 we discuss the constraints on the dust properties such as porosity, sizes and density distribution given by our model. The gas species of cometary origin and the silicate mineralogy are also discussed. The conclusion is given in Sect. 6.

2. Dust properties

Based on the observational evidence already mentioned in Sect. 1, we propose that the dust particles in the β Pictoris disk are of cometary origin. We adopt the comet dust model of Greenberg (1982, 1998) of which the basic idea is that, comet dust grains are fluffy aggregates of primitive interstellar dust. Interstellar dust consists of a silicate core, an organic refractory material mantle resulting from ultraviolet photoprocessing of ice accreted on the silicate core, and an additional H_2O dominated ice mantle accreted in dense molecular clouds and in the final stage of contraction of the protostellar nebula cloud (Greenberg 1978). Comets form through the aggregation of the dust grains in protostellar clouds with all the primitive material properties remaining essentially unaltered. It is natural to assume that the comets in the β Pictoris disk which act as the dust source formed out of the same protostellar nebula as the central star β Pictoris. When these comets come close to the star, some comet dust particles are sputtered out and stay in the disk. Exposed to the radiation in the inner disk, say, within ~ 100 AU, the dust grains could be heated to well above 120 K and so that the outer ice mantles would evaporate, leaving the disk dust grains as fluffy silicate core-organic refractory mantle aggregates. Deeper into the inner region of the disk, the dust temperatures are so high that some of the organic refractory mantles also evaporate and some silicates are even crystallized. The strong radiation pressure blows the small particles out, so that the crystalline silicate particles become distributed over the entire disk. While in the outer disk, say ≥ 100 AU, the grain temperatures could be lower than 120 K, thus it is possible that water vapor recondenses on the individual particles of the aggregates. The recondensation of water vapor not only modifies the chemical composition but also reduces the porosity (less empty space) of the aggregate. It is also possible that some comets which have never come close enough to β Pictoris, also contribute a certain amount of dust particles through shattering and collision. The dust particles originating from such processes naturally keep their original ice mantles.

2.1. Dust materials

One conclusion drawn from the preceding discussion is that there are two main kinds of dust grains in the β Pictoris disk: **a** – porous aggregates of amorphous silicate core-organic refractory mantle (without/with ice mantle) interstellar dust; **b** – porous aggregates of crystalline silicate (without/with ice mantle). In reality, definitely some dust particles evaporate their organic refractory mantles partially and the amorphous silicate cores are only partially crystallized. However, for simplicity, we group all these particles in the two extreme cases **a** and **b**.

As far as grain material properties are concerned, we concentrate on the optical properties of the various dust components which are described in terms of their optical constants (complex indices of refraction) $m(\lambda) = m^{'}(\lambda) - i\,m^{''}(\lambda)$. The optical constants of amorphous silicate and organic refractory materials have been discussed in detail by Li & Greenberg (1997). Here we focus on crystalline silicate and ice.

In order to study the fine structures of silicate bands, in particular, to compare the predicted silicate features with the observations, we need not only high resolution data of the optical constants in the NIR/MIR range but also a complete set of data from the far ultraviolet (FUV), through visual to the FIR for various chemical compositions since the absorption of radiation from β Pictoris occurs mostly in the near ultraviolet and visual while the emission occurs in the MIR and FIR. However, the optical constants have been measured only for samples with a limited chemical variety and for a limited wavelength range. Therefore it is necessary to construct a set of optical constants over a wide range of wavelengths on the basis of the existing experimental data and some reasonable assumptions. For $\lambda \leq 0.3\,\mu m$, we have taken the imaginary part of the refraction index $m^{''}(\lambda)$ of crystalline olivine measured by Huffman & Stapp (1973). For the range $0.3\,\mu m \leq \lambda \leq 6\,\mu m$, the $m^{''}(\lambda)$ of Draine & Lee (1984) have been adopted. In the range of $7\,\mu m \leq \lambda \leq 200\,\mu m$, Mukai & Koike (1990) have measured the transmission spectrum of crystalline olivine ($(Mg_{0.9}Fe_{0.1})_2SiO_4$) and from that they derived 17 Lorentz oscillators. We have calculated the index of refraction of crystalline olivine from 7 to 200 μm using the Lorentz oscillator dispersion parameters given by Mukai & Koike (1990). For the FIR ($\lambda \geq 200\,\mu m$), the absorption of crystalline materials is dominated by free electrons and falls off as λ^{-2} (Tielens & Allamandola 1987), thus we assume $m^{''}(\lambda) \propto \lambda^{-1}$ which indicates that the FIR absorption is $\propto \lambda^{-2}$. The imaginary parts of the refraction indices $m^{''}(\lambda)$ are then smoothly joined from the FUV to the millimeter region. Finally, the real parts of the optical constants $m^{'}(\lambda)$ are calculated from $m^{''}(\lambda)$ by using the Kramers-Kronig relation. The effects of different crystalline silicate minerals on the model spectra will be demonstrated in Sect. 5.

Obviously, the cometary ices are a mixture of H_2O, CO, CO_2, CH_3OH, H_2CO etc. Since H_2O ice is the dominant component, and since we are not interested in the detailed structure of ice bands, we employ the optical constants of H_2O ice. The experimental data on $m(\lambda)$ for H_2O ice ranging from the FUV to the FIR are also poor. The following procedure was used to

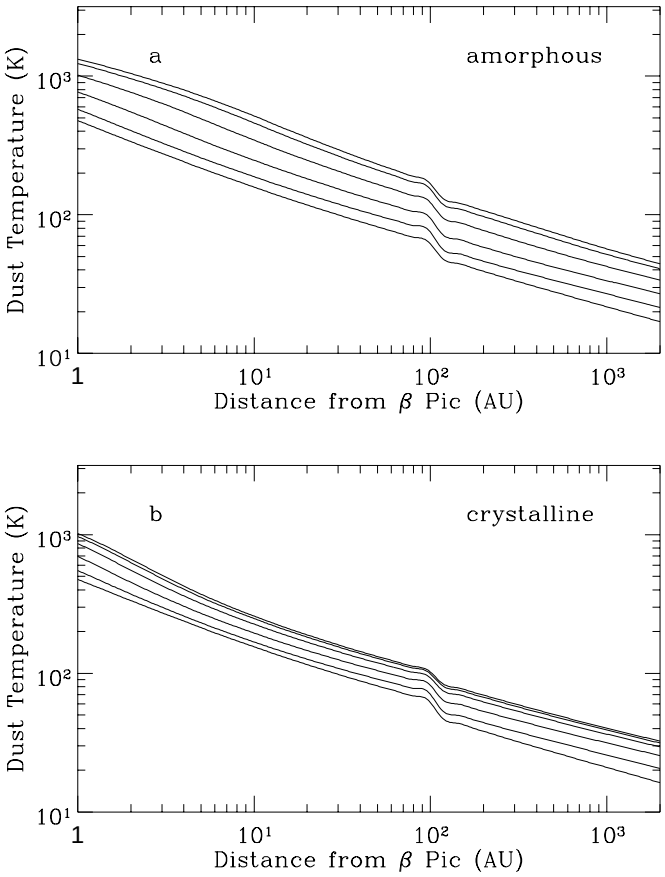

Fig. 1. The radial temperature distribution of porous aggregates with a porosity of P = 0.975 and masses of $10^{-14}, 10^{-12}, ...10^{-4}\ g$ (from top to bottom) for a) the amorphous silicate model – fluffy aggregates of amorphous silicate core-organic refractory mantle (with an outer ice mantle at $r > 100$ AU) particles and b) the crystalline silicate model – fluffy aggregates of crystalline silicate (with no organic mantle but with an outer ice mantle at $r > 100$ AU) particles (see text of Sect. 4).

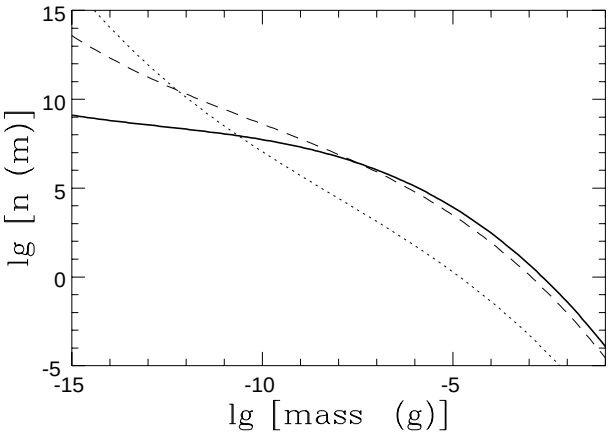

Fig. 2. The mass distributions of dust grains in the inner region $[r_{inner}, r_1]$ (dotted line), the middle region $[r_1, r_2]$ (dashed line), the outer region $[r_2, r_{outer}]$ (solid line). The small particles in the inner disk are highly enhanced. The mass distribution of the outer region is the same as that of comet Halley dust.

construct a complete set of optical constants. First, we adopt the laboratory data ($m''(\lambda)$) of 10 K pure H_2O ice in the range of $2\,\mu m \leq \lambda \leq 200\,\mu m$ (Hudgins et al. 1993). For $\lambda \leq 2\,\mu m$ we use the $m''(\lambda)$ of crystalline H_2O ice (Greenberg 1968). For FIR ($\lambda \geq 200\,\mu m$) we assume that $m''(\lambda)$ falls off as λ^{-n} with n in the range of 0.0 to 1.0. Finally the imaginary parts $m''(\lambda)$ are smoothly connected from the FUV to the millimeter and the real parts $m'(\lambda)$ are then calculated from $m''(\lambda)$ by using the Kramers-Kronig relation. Note that both amorphous and crystalline ice materials could be present in the outer disk region. The ices resulting from the recondensation of water vapor are predicted to be crystalline (Kouchi et al. 1994) while the primitive ice materials are in an amorphous phase, but for the purpose of this work (only the dust emission is of concern) there would be no significant differences between using crystalline ice and amorphous ice since the temperatures for these materials are similar, as shown by Mukai & Mukai (1984).

The position in the disk where the ice mantle first occurs (in other word, the ice sublimation boundary) depends on the grain materials and sizes. For small particles the presence of an ice mantle occurs farther out than for large particles since small particles are hotter than large particles with the same composition. On the other hand, the aggregates of core-mantle particles are more absorbing than the aggregates of crystalline silicate particles so that the presence of ice mantles is further removed outward. Indeed the ice sublimation boundaries cover a wide range of disk radii as one can see from the grain temperature distribution as plotted in Fig. 1a,b (see Sect. 4). However, for simplicity, we will assume that the presence of ice mantles occurs at the same distance from the central star; namely, we choose an intermediate value in the sublimation boundary range as the sublimation boundary for all the grains.

2.2. Dust size (mass) distribution

As discussed in Sect. 1, the earlier works on β Pictoris yielded widely ranging different values for the grain size. It is difficult to constrain grain size without taking into account both the silicate spectra and the continuum emission. Here we are neither going to adopt a power law distribution which was taken as granted by other models (e.g., Backman et al. 1992, Knacke et al. 1993), nor are we going to employ the Hanner size distribution form (Hanner et al. 1985). We shall assume as a first approximation that the dust grains in the β Pictoris disk have a size distribution similar to that of comet Halley. Although we cannot say that this need be exactly the case in the β Pictoris system, it is considered as a reasonable starting point if we believe that the dust is shed by comets. The spacecrafts Vega 1, Vega 2 and Giotto performed in situ measurements of dust mass distributions when approaching close to comet Halley (see Fig. 3a in Greenberg & Hage 1990). A mass distribution can be converted into a size distribution provided one has knowledge of the grain mass density and morphology. In this work, the mass densities of silicate, organic refractory and ice are assumed to be $\rho_{si} = 3.5\,g\,cm^{-3}$, $\rho_{or} = 1.8\,g\,cm^{-3}$, $\rho_{ice} = 1.2\,g\,cm^{-3}$, respectively.

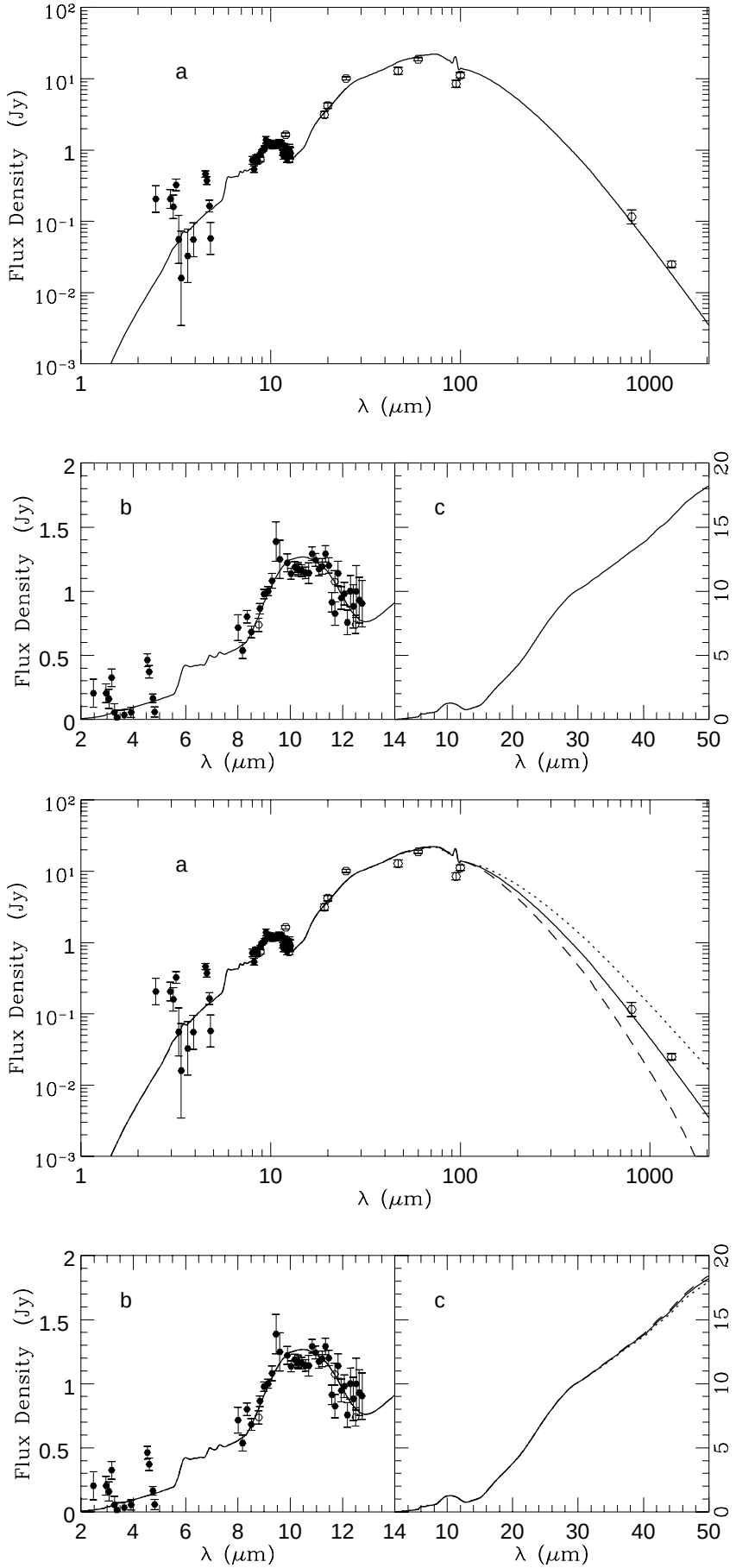

Fig. 3a–c. The spectral energy distribution predicted from the amorphous silicate model with a porosity of P = 0.975 together with various observational data as summarized in Sect. 4. The grain size distributions are those of Fig. 2. The imaginary part of the refractive index of ice grains falls off as $m''_{ice}(\lambda) \propto \lambda^{-0.5}$ in the FIR. The dust volume number density goes as $n(r) \propto r^{-2.7}$ in the entire disk. For illustrative purposes, the NIR and the 10 μm silicate emission spectra are presented in **b** with the MIR spectra in **c** in addition to the overall spectral energy distribution from the NIR to the millimeter plotted in **a**.

Fig. 4a–c. The spectral energy distributions obtained from three dust models with $m''_{ice}(\lambda) \propto \lambda^{-0.0}$ (dotted line), $m''_{ice}(\lambda) \propto \lambda^{-0.5}$ (solid line), and $m''_{ice}(\lambda) \propto \lambda^{-1.0}$ (dashed line) in the FIR. The other parameters are identical to those of Fig. 3.

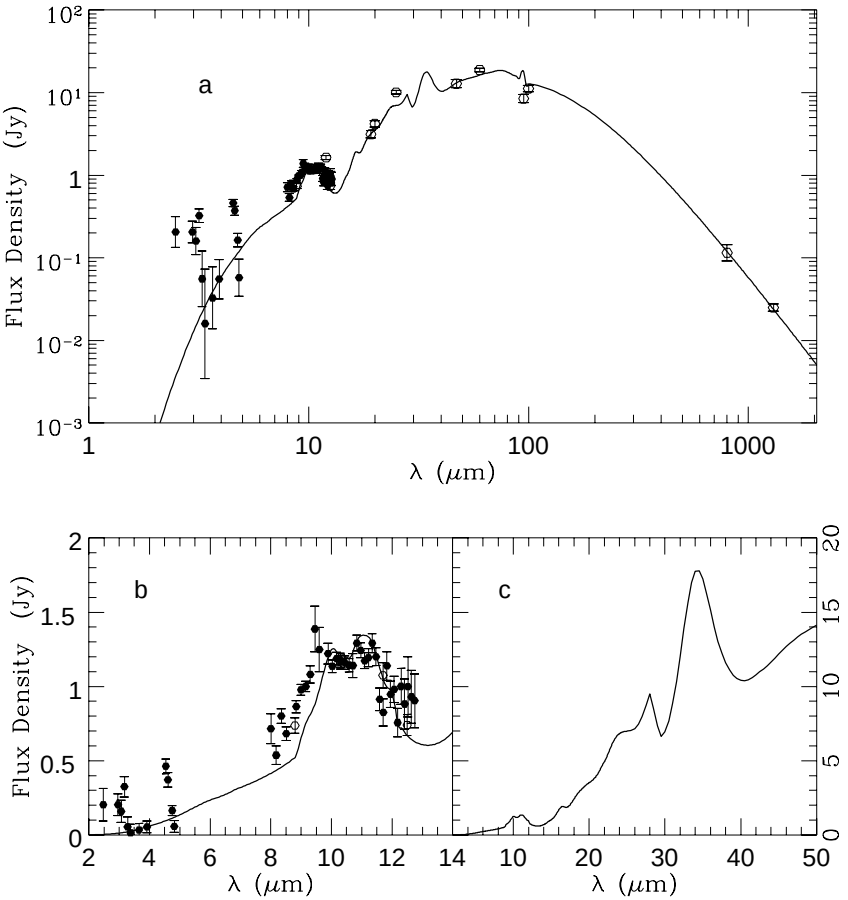

Fig. 5a–c. Same as Fig. 3 except for the crystalline silicate model.

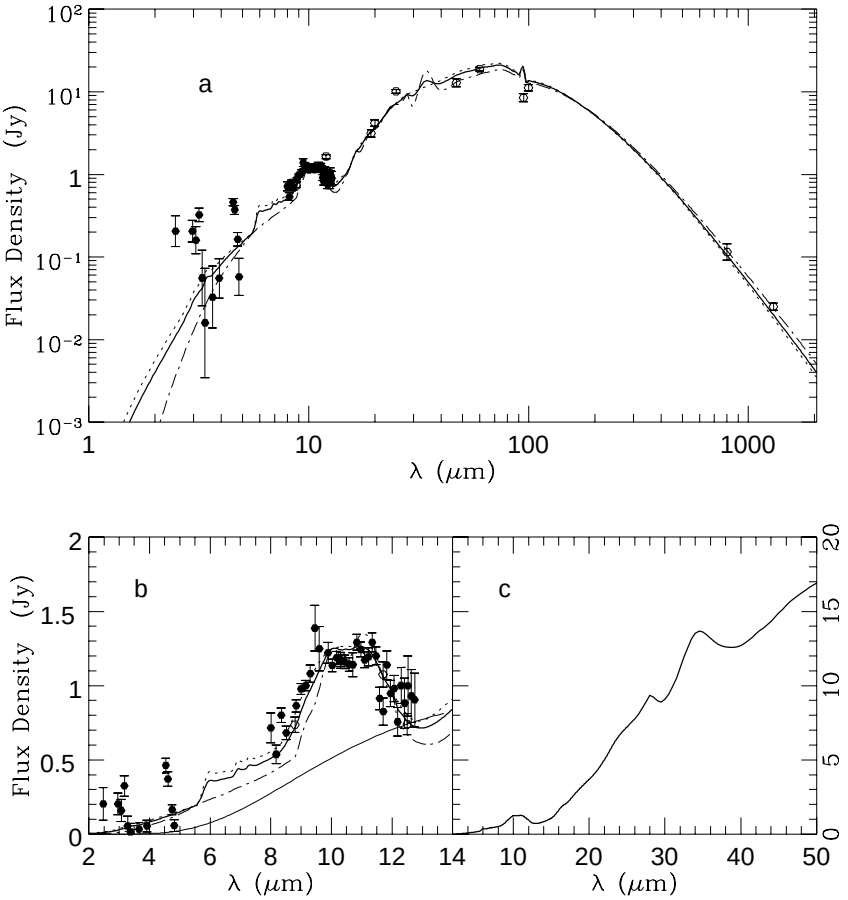

Fig. 6A. The spectral energy distribution derived from a mixture of the amorphous silicate model (dotted line; same as Fig. 3) and the crystalline silicate model (dot-dashed line; same as Fig. 5) with an assumption of 20% crystalline silicates. **a** The overall spectrum from the NIR to the millimeter; **b** The 10 μm silicate feature; **c** The MIR emission bands.

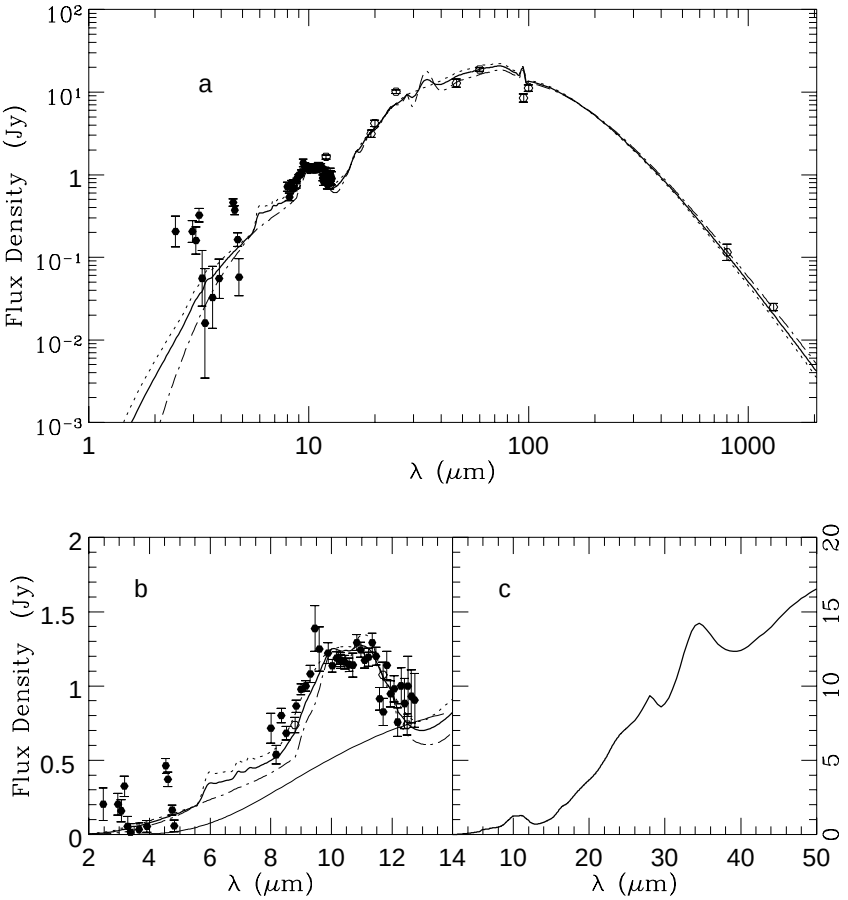

Fig. 6B. Same as Fig. 6A except for 30% crystalline silicates.

Table 1. The spatial distribution of dust grains and the total dust mass. (If a newly determined β Pictoris distance 19.28 pc rather than 16.6 pc is adopted, the radial distance r should increase by $\approx$ 16%, and the dust mass should be multiplied by a factor of $\approx$ 1.35.)

Materials	P*	β, $(n(r) \propto r^{-\beta})$			Dust Mass (g)			
		[1, 40] AU	[40, 100] AU	[100, 2200] AU	[1, 40]	[40, 100]	[100, 2200]	[1, 2200]
am†	0.975	2.7	2.7	2.7	5.67×10^{22}	6.12×10^{25}	2.19×10^{27}	2.25×10^{27}
cryst‡	0.975	2.7	2.7	2.7	2.40×10^{22}	5.60×10^{25}	1.97×10^{27}	2.03×10^{27}
am	0.975	1.8	2.7	2.7	3.65×10^{23}	5.25×10^{25}	1.88×10^{27}	1.93×10^{27}
cryst	0.975	1.8	2.7	2.7	2.17×10^{23}	5.30×10^{25}	1.87×10^{27}	1.92×10^{27}
am	0.975	1.8	1.8	2.7	3.81×10^{23}	6.98×10^{25}	2.37×10^{27}	2.44×10^{27}
cryst	0.975	1.8	1.8	2.7	2.37×10^{23}	6.95×10^{25}	2.32×10^{27}	2.39×10^{27}
am	0.975	2.0	2.0	2.7	2.47×10^{23}	5.58×10^{25}	2.03×10^{27}	2.09×10^{27}
cryst	0.975	2.0	2.0	2.7	1.40×10^{23}	5.43×10^{25}	1.94×10^{27}	1.99×10^{27}
am	0.95	2.7	2.7	2.7	9.60×10^{22}	1.07×10^{26}	2.63×10^{27}	2.74×10^{27}
cryst	0.95	2.7	2.7	2.7	4.30×10^{22}	1.02×10^{26}	2.46×10^{27}	2.56×10^{27}

* porosity; † the amorphous silicate model; ‡ the crystalline silicate model.

For comet Halley dust, it has been deduced both observationally (Vaisberg et al. 1986) and theoretically (Thomas & Keller 1989; Greenberg & Li 1997) that large porous aggregates sequentially fragment into smaller ones due to sublimation effects and/or grain-grain collisions when they move outward in the coma. Thus the size distribution for smaller particles should be enhanced relative to larger particles. For β Pictoris, the enhancement effect may be more significant than for comet Halley due to the stronger stellar radiation (more efficient sublimation) and denser dust environment (more efficient collisions). The Halley dust size distribution was represented by a polynomial function. The enhancement of smaller grains can be achieved by adjusting the coefficients.

2.3. Dust spatial density distribution

We assume that the dust density distribution follows a power law: $n(r) \propto r^{-\beta}$, where r is the distance from the central star,

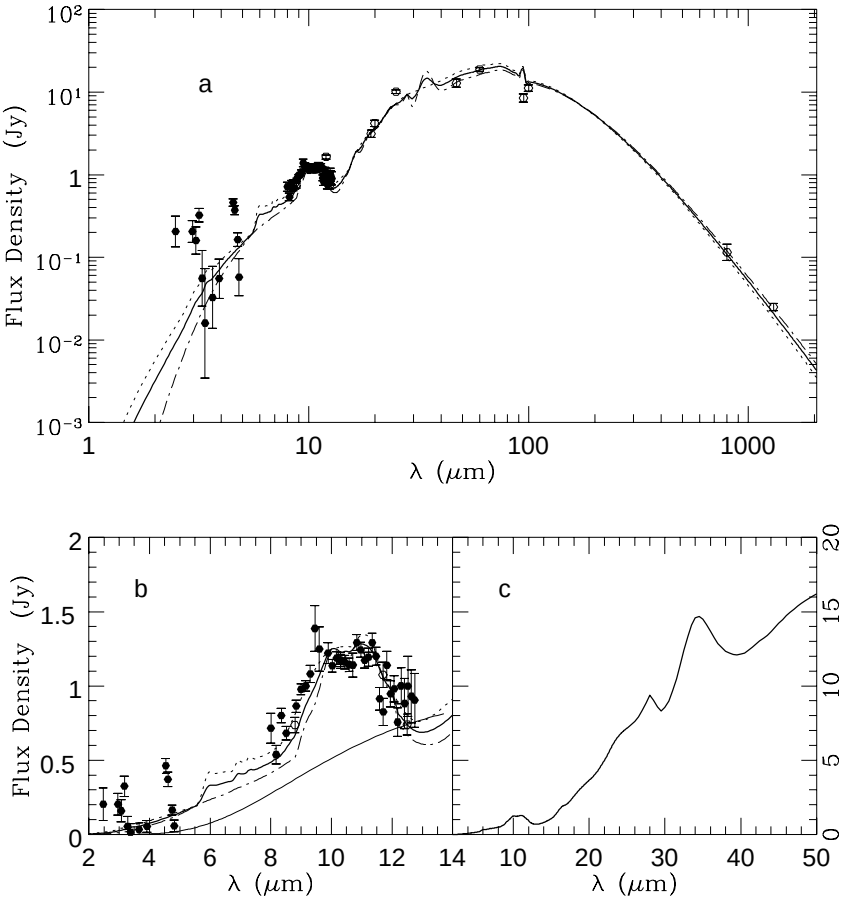

Fig. 6C. Same as Fig. 6A except for 40% crystalline silicate.

$n(r)$ is the volume number density. We also assume that the disk is circularly symmetric, perfectly wedge-shaped with the disk thickness proportional to the radius r and a constant opening angle. Strictly speaking, these assumptions are not completely valid because observations do show some asymmetry (Lagage & Pantin 1994; Kalas & Jewitt 1995). Artymowicz et al. (1989) derived $\beta \approx 2.7$ for $r \geq 100$ AU from their modeling of scattered optical light. Following Artymowicz et al. (1989), we adopt $\beta \approx 2.7$ for the outer region of the disk plane ($r \geq 100$ AU). For the inner region, we keep β as a free parameter. We note that the dust density distribution cannot be uniquely determined because it is coupled with the grain size (mass) distribution. Further discussion will be given in Sect. 5.

3. The modeling methods

In order to model the spectral energy distribution and the spectral features, we need to know the absorption and emission properties of the emitters and their steady state temperatures.

The absorption efficiency $Q_{abs}(a, \lambda)$ is obtained from Mie theory, assuming both the porous aggregate and the individual particles in the aggregate are spherical. For $\lambda \geq 1\,\mu m$, the Maxwell-Garnett effective medium theory (Maxwell-Garnett 1904; Bohren & Huffman 1983) is applied twice, as in Greenberg & Hage (1990), to calculate the effective dielectric function first of the individual core-mantle particles and then of the aggregates. For the aggregates in which the individual particles have an additional icy coat, the effective medium theory should be applied three times. For $\lambda < 1\,\mu m$, the aggregate is approximated as a cloud of independent particles. A detailed description of the method of calculation has been given by Greenberg & Hage (1990) and Hage & Greenberg (1990).

The dust temperatures can then be calculated on the basis of the dust energy balance,

$$\omega \int_0^\infty \pi a^2 Q_{abs}(a,\lambda) 4\,\pi\, B(T_\star, \lambda)\, d\lambda = \int_0^\infty \pi\, a^2\, Q_{abs}(a,\lambda) 4\,\pi\, B[T_d(r,a), \lambda]\, d\lambda \quad (1)$$

where ω is the dilution factor, $\approx (\frac{R_\star}{2r})^2$; $T_\star$ (≈ 8200 K) and $R_\star$ ($\approx 6.23 \times 10^{-3}$ AU) are the temperature and radius of the central star, respectively; $B[T_d(r,a), \lambda]$ is the Planck function. Here the stellar flux is approximated by a blackbody at temperature $T_\star$. The grain temperature $T_d(r,a)$ is a function of a (grain size, mass), of r (the distance from the location of the grain to the central star), and, of course, of grain materials.

The disk is assumed to be circularly symmetric, wedge-shaped. The opening angle of the wedge is assumed constant so that the disk thickness is proportional to the radius, $h(r) = l_0\, r$.

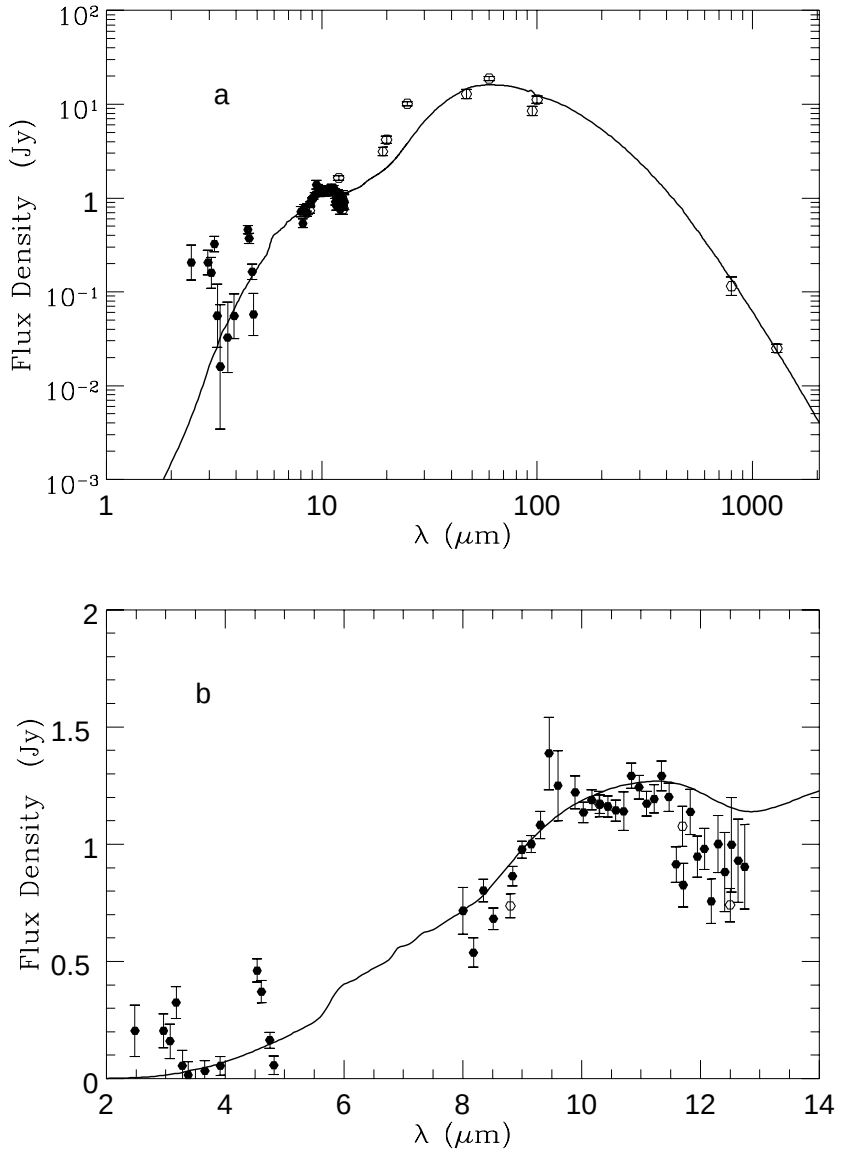

Fig. 7A. The spectral energy distribution calculated for the amorphous silicate model with a porosity of P = 0.85. The dust volume number density falls off as $n(r) \propto r^{-2.7}$ in the entire disk. **a** The overall spectral energy distribution from the NIR to the millimeter; **b** The 10 μm silicate emission spectrum.

The flux density emitted by the disk received at the Earth is given by

$$F(\lambda) = \int_{r_{inner}}^{r_{outer}} \int_{a_-}^{a_+} \pi a^2 Q_{abs}(a,\lambda) n(a) \times B[T_d(a,r),\lambda]\, da\, n(r) l_0\, r\, \frac{2\pi r dr}{D^2} \quad (2)$$

where n(a) is the dust size distribution and n(r) is the dust volume density distribution; D ($\sim$ 16.6 pc) is the distance from the Earth to β Pictoris; r_{inner} and r_{outer} are the inner and outer boundaries of the disk, respectively. Most recently, based on the Hipparcos satellite measurements of the β Pictoris parallax, Crifo et al. (1997) evaluated a new distance, $D' \simeq 19.28 \pm 0.19$ pc, $\approx$ 16% higher than the commonly adopted one (D $\simeq$ 16.6 pc). This would increase the stellar luminosity by $(D'/D)^2 - 1$ ($\approx$ 35%), and the star radius by D$'$/D-1 ($\approx$ 16%). Before the confirmation of this new determination, and for the convenience of comparing our results with those of the earlier works, we shall still adopt the previous stellar parameters (D $\simeq$ 16.6 pc, $R_\star \approx 6.23 \times 10^{-3}$ AU). We note that introducing the new distance D$'$ does not change the basic conclusions. All that need be modified are just the geometrical dimensions and dust mass. More detailed discussion of this will be presented in Sect. 5.2.

In the earlier works (e.g., Backman et al. 1992, Knacke et al. 1993, Harvey et al. 1996) the disk was divided into two components with a boundary at $\sim$ 80 AU. The two components are different in both grain sizes and grain density distributions. The most noteworthy point of their disk structure is the sudden jump of the grain number density at the boundary (80 AU). They attributed this to the sublimation of pure icy particles in the inner component. It seems to us more consistent to imagine that the volatile ices accompany the refractories as mantles than that they are isolated from the refractories and form pure ice grains. Thus the sublimation of ices may indeed lead to a change in the grain sizes, but a sudden jump where sublimation stops does not appear at all reasonable in terms of the comet dust hypothesis. Such jump might be conceived only if the silicate and ice particles are separate components. This appears highly improb-

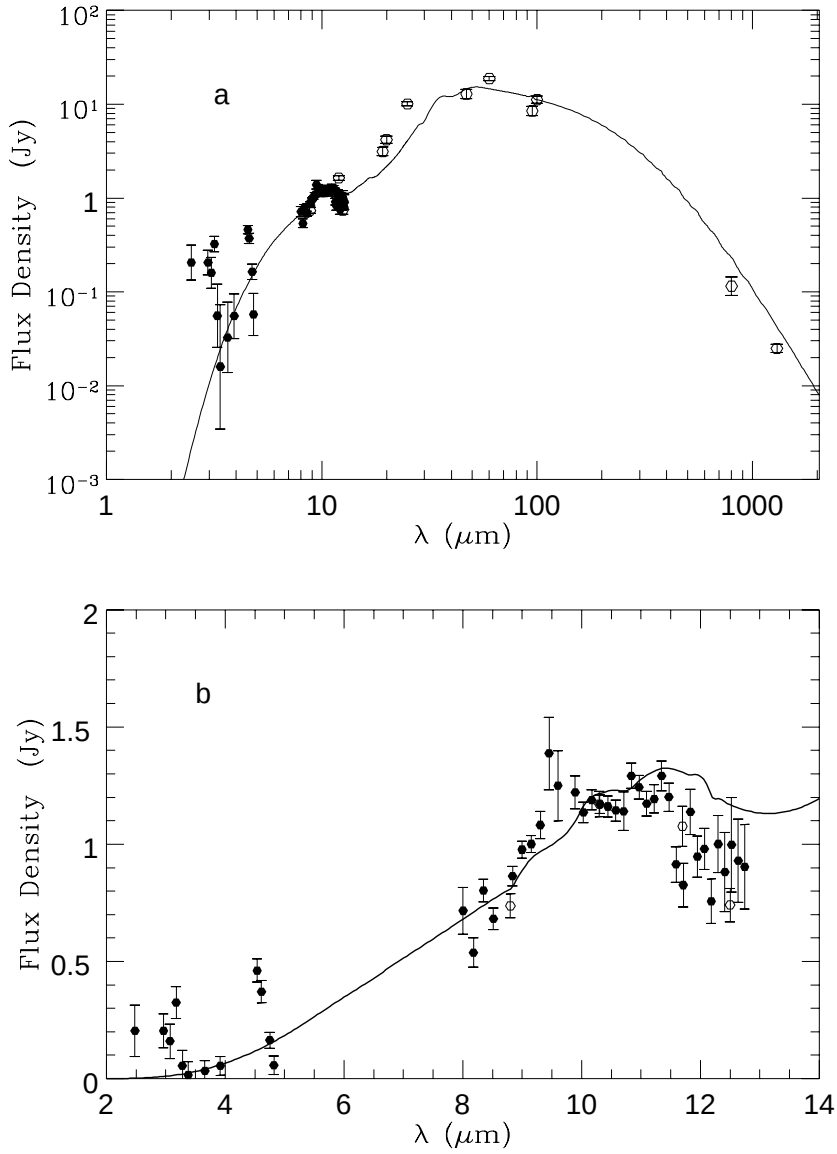

Fig. 7B. Same as Fig. 7A but for the crystalline silicate model.

able. Artymowicz (1994) also questioned the sudden jump of grain density in terms of the albedo and the widely ranging ice sublimation boundary.

We have chosen to divide the disk into three components: 1) an inner component between r_{inner} and r_1 ($r \in [r_{inner}, r_1]$) – in which the dust grains contribute to the NIR and the 10 μm silicate emission ($\lambda < 20\mu m$); 2) a middle component between r_1 and r_2 ($r \in [r_1, r_2]$) – in which the dust grains contribute to the mid-infrared emission ($20 < \lambda < 60\mu m$); 3) an outer component between r_2 and r_{outer} ($r \in [r_2, r_{outer}]$) – in which the dust grains contribute to the FIR and millimeter emission. Although the 10 μm silicate emission is dominated by the inner component particles, the particles in the $[r_1, r_2]$ region have an effect on the long wavelength wing, thus the silicate spectra as well as the MIR emission define r_1. The disk radius, r_2, where the icy mantles first appear is chosen to be $\sim$ 100 AU, an intermediate value in the sublimation boundary range.

To model the spectral energy distribution, we need to know:

1. *The mass (volume) ratio of the organic refractory mantle to the silicate core*, M_{or}/M_{si}. We note that the value of M_{or}/M_{si} could be highly variable for different astrophysical environments (diffuse clouds, dense molecular clouds, comet, etc). The mass spectra of comet Halley dust as measured by the PUMA mass spectrometer on board the spacecraft Vega 1 indicated that $M_{or}/M_{si} \approx 1$ (Kissel & Krueger 1987). In this work, we adopt $M_{or}/M_{si} = 1$.

2. *The mass (volume) ratio of the ice mantle to the silicate core-organic refractory mantle, M_{ice}/M_{si+or}*. Recently, Greenberg (1998) has developed a model of comet nucleus in which the chemical composition is very precisely constrained by combining the latest knowledge of interstellar dust, the solar system elemental abundances, the dust composition of comet Halley, and the latest data on the volatile molecules of comet comae. It gives $M_{ice}/M_{si+or} \approx 1$ if all the volatile molecules and small carbonaceous particles as well as PAH's are accreted into the

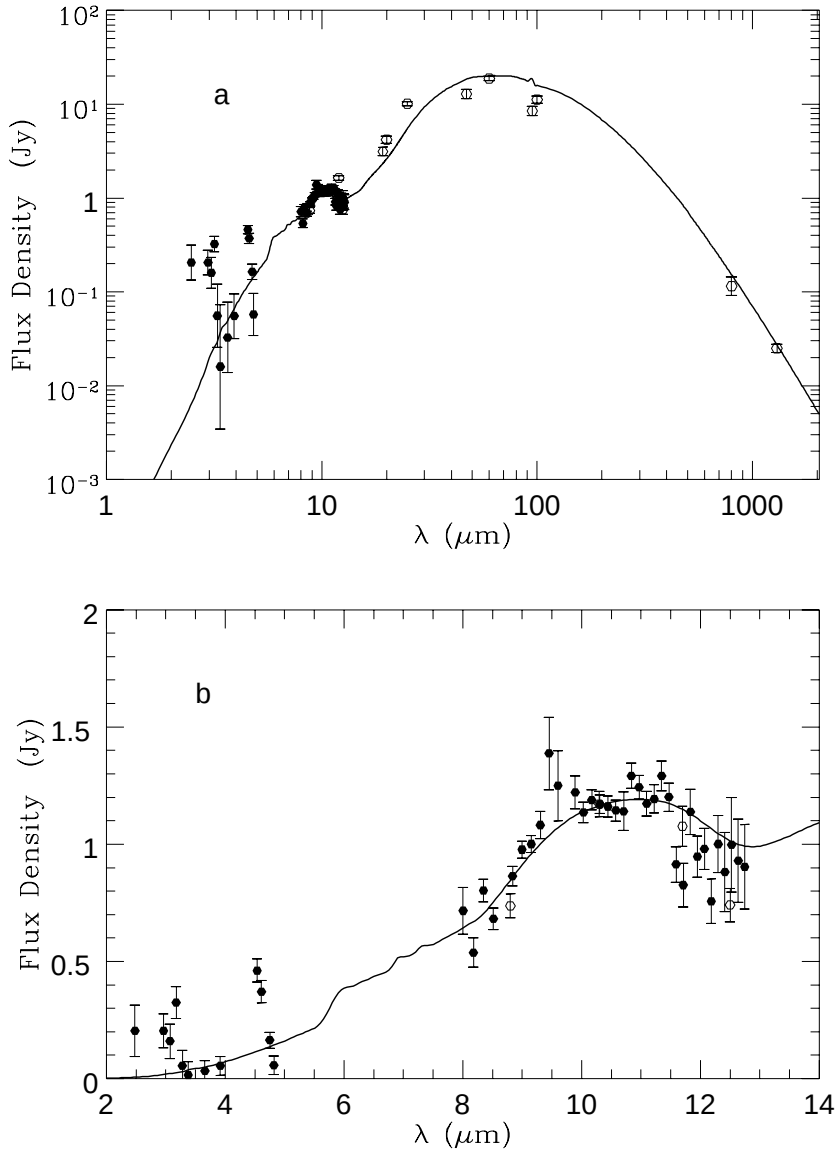

Fig. 8A. Same as Fig. 7A but with a porosity of P = 0.90.

H_2O ice mantle. So, we assume $M_{ice}/M_{si+or} = 1$ for the aggregates of ice coated interstellar grains noting that the ice here is really about 75% H_2O, the rest being CO, CO_2 etc. (Greenberg 1998).

3. *The porosity P*. For comet Halley dust, Greenberg & Hage (1990) have shown that the dust grains must be very fluffy with a porosity in the range of $0.93 \leq P \leq 0.975$ in order to get the silicate excess emission. High porosity is also required to explain the extended CO emission in the coma of comet Halley (Greenberg & Li 1997). In this work we consider a wide range of porosities, but as will be shown in Sect. 5, one finds that the porosity is actually well constrained to a rather narrow range.

4. *The grain size (mass) distribution n(a)*. In the inner region of the disk, the grain size distribution in combination with porosity is well constrained by the silicate spectral feature. We point out here that the distribution of small particles must be enhanced (relative to the Halley size distribution) otherwise either there is too little MIR, FIR emission (in the case of high porosity, say, P = 0.975) or there is no silicate emission feature at all (in the case of low porosity). Our model calculations also imply that the particles responsible for the MIR emission must also have an enhancement in the small particles. The lower mass limit was set at $10^{-14}\,g$ which is equivalent to an individual tenth micron interstellar grain. Particles with radii smaller than tenth micron contribute very little to the thermal emission in comet Halley (Hanner et al. 1987). The upper mass limit was set at $10^{-3}\,g$. This upper mass limit is high enough since such high mass particles are so cold that their thermal emission is negligible.

5. *The grain density distribution*. As we will see in the discussion in Sect. 5, $n(r)$ is not uniquely determined but coupled with the grain mass distribution.

6. *The inner and outer boundary of the disk, r_{inner} and r_{outer} (also r_1, r_2)*. There is a large scatter among the values of r_{inner} adopted for the previous models. The best fit model by Backman et al. (1992) gave r_{inner} = 4.5 AU; and that by Chini

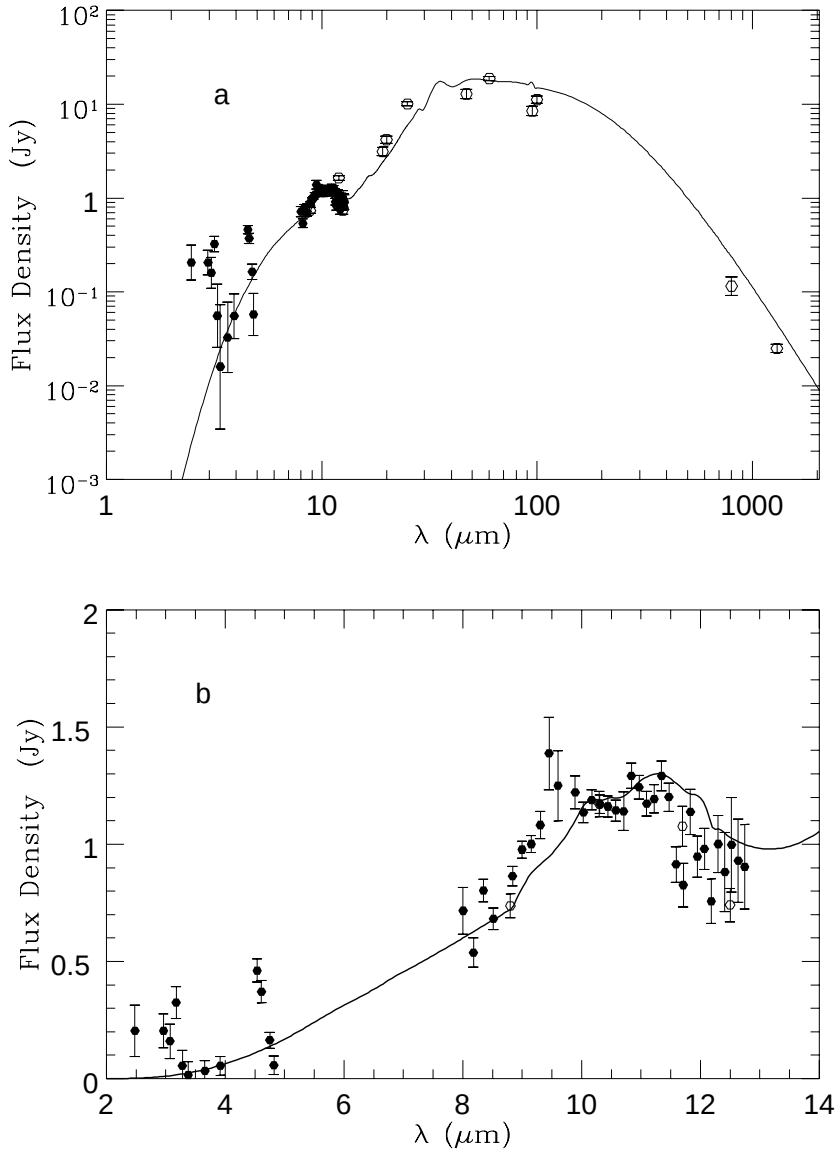

Fig. 8B. Same as Fig. 8A but for the crystalline silicate model.

et al. (1991) r_{inner} = 36 AU; while that by Harvey et al. (1996) gave r_{inner} = 5.0 AU. As discussed in Sect. 1, since the dust grains in the models of Backman et al. (1992) and Chini et al. (1991) are so far away from the central star, even the smallest particles cannot be heated enough to radiate with a silicate excess emission. Our model calculations show that $r_{inner} \approx 1$ AU is the best value for the inner boundary. For r_{inner} much less than 1 AU, the particles will be heated to such high temperatures that they would be completely evaporated. On the other hand, for r_{inner} = 5 AU, even in the case in which small particles are greatly enhanced, the particles are still not hot enough to give the silicate emission. Even for r_{inner} = 3 AU, the silicate feature is either too shallow or peaks at the wrong wavelength. It is interesting to note that Knacke et al. (1993) also found that among their various models $r_{inner} \approx 1$ AU provides the best fit to the silicate feature. Consequently we believe that the inner boundary is rather strictly constrained by the silicate excess emission requirement. The outer boundary of the disk extends to $>$ 2000 AU (Smith & Terrile 1987). Our model calculations show that the difference of the 1300 μm emission is rather weakly dependent on the choice of the outer radius: the difference between the models using r_{outer} = 1600 AU and r_{outer} = 2500 AU is only about 5%, well within the uncertainties of the millimeter observations since the dust grains in the outer region ($r > 2000$ AU) are too cold even to contribute much to submillimeter/millimeter emission. We have chosen r_{outer} = 2200 AU.

4. The spectral energy distribution: dust sizes and optical properties

The observational data with which we compare our theoretical results are the intermediate resolution infrared spectra (the silicate spectra) at 2.6 – 13.5 μm of Knacke et al. (1993), the spectrophotometry of Telesco & Knacke (1991) at 8.8, 10.3, 11.7 and 12.5 μm, and the photometry of Backman et al. (1992) at

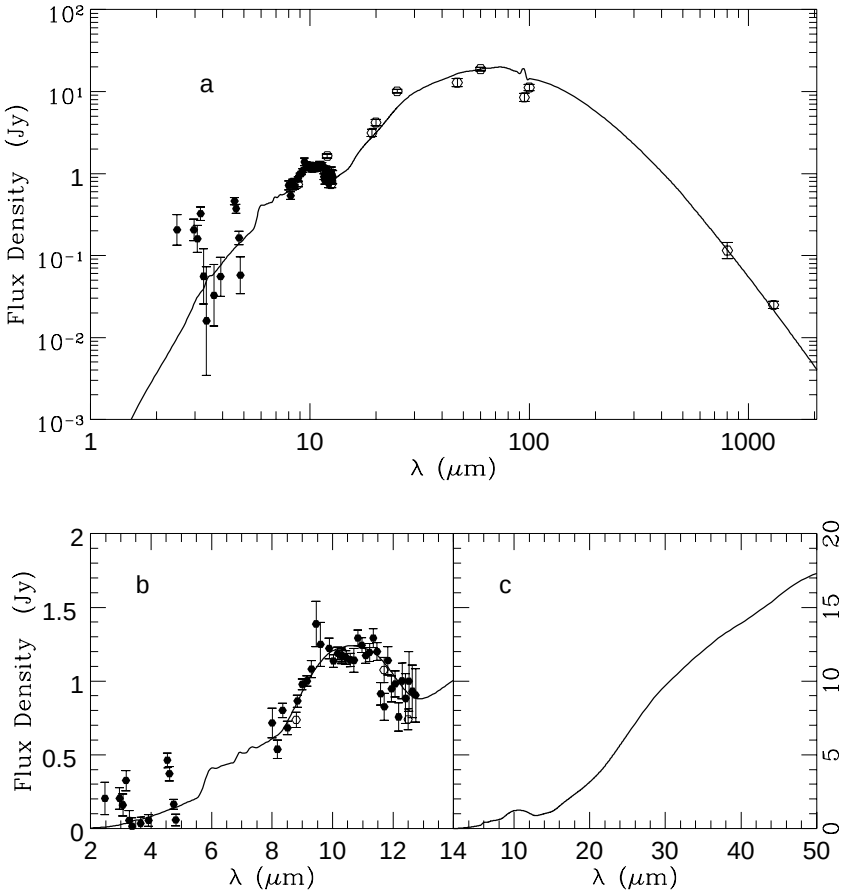

Fig. 9A. The spectral energy distribution obtained from the amorphous silicate model with a porosity of P = 0.95. The dust volume number density falls off as $n(r) \propto r^{-2.7}$ in the entire disk. The grain size distributions are presented in Fig. 9D.

3.45, 4.80, 10.1 and 20 μm, of Telesco et al. (1988) at 10 and 20 μm, of the IRAS survey at 12, 25, 60 and 100 μm, of the KAO (the Kuiper Airborne Observatory) at 47 and 95 μm (Harvey et al. 1996), of Zuckerman & Becklin (1993) at 800 μm, and of Chini et al. (1991) at 1300 μm. Note these measurements were made at different beam sizes.

Once the grain properties (M_{or}/M_{si}, M_{ice}/M_{si+or}, P, grain sizes) are specified, the absorption efficiencies $Q_{abs}(a, \lambda)$ can be derived. The grain temperatures can then be obtained from Eq. 1. Here we first consider an amorphous silicate model and then a crystalline silicate model.

In Fig. 1a we plot the temperatures as a function of the distance from the central star for the aggregates of amorphous silicate core-organic refractory mantle (with an ice mantle at $r > 100$ AU) grains with $M_{or}/M_{si} = 1$, $M_{ice}/M_{si+or} = 1$, P=0.975 and various masses. It is apparent in Fig. 1a that the temperature decreases with the increase of grain size. At $r_2 = 100$ AU the presence of ice mantles makes the particles more transparent and thus leads to lower temperatures. In the inner several AU of the disk, some dust grains are heated to above 1000 K. Note that laboratory studies show that amorphous silicate can be annealed when heated to $\sim 700 - 1200$ K; for example, amorphous magnesium silicate was converted to crystalline olivine by heating to 1270 K for one hour (Day & Donn 1978). Glassy silicate particles can be crystallized by heating to 875 K for 105 hours (Koike & Tsuchiyama 1992). This implies that the crystallization of amorphous silicate could occur in this region.

Following the discussion in Sect. 3, we adopt $M_{or}/M_{si} = 1$, $M_{ice}/M_{si+or} = 1$, $r_{inner} = 1$ AU, $r_{outer} = 2200$ AU. The grain number density $n(r)$ is assumed to be $\propto r^{-2.7}$ over the entire disk with $r_2 = 100$ AU. We first consider a high porosity P=0.975 as proposed by Greenberg & Hage (1990) and Greenberg & Li (1997). The effects of different grain density distributions and porosities will be discussed in Sect. 5. We then adjust the grain size (mass) distributions of the three disk components so as to match both the silicate feature, the mid-infrared and the FIR/millimeter emission. Our model calculations show that the smaller particles in the inner component of the disk should be greatly enhanced, those of the middle component of the disk moderately enhanced, while the outer disk has the same size distribution as that of comet Halley dust. r_1 is well constrained to be ≈ 40 AU by fitting the silicate feature and the mid-infrared emission. The resulting grain mass distributions are presented in Fig. 2. Note that for a more realistic case the dust size distribution should be spatial dependent. Here the spatial dependence has been simplified by adopting three distributions each of which represents the average size distribution of one disk component. Fig. 3a shows the theoretical spectral energy distribution as well as the observations from the NIR to the FIR/millimeter. The 10 μm silicate feature and the MIR spectra are illustrated in Fig. 3b and Fig. 3c, respectively. Fig. 3 demon-

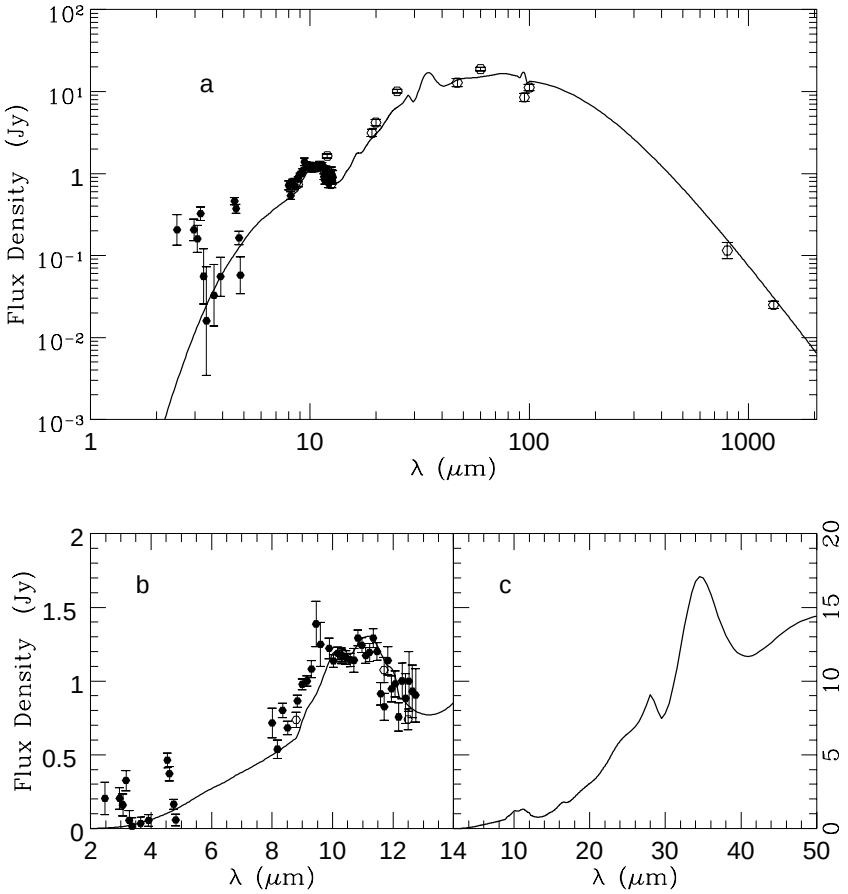

Fig. 9B. Same as Fig. 9A but for the crystalline silicate model.

strates that the amorphous silicate model (porous aggregates of amorphous silicate core-organic refractory mantle without/with an additional ice coat) provides a good match to the continuum from NIR to FIR/millimeter as well as the silicate spectrum except for the 11.2 μm crystalline silicate feature which will be modeled below. The sudden jump at $\sim$ 5 μm is due to the various C=C, C=O, C-OH, C$\equiv$N, C-NH_2 etc. stretches in the organic refractory materials (Greenberg et al. 1995). One can see from Fig. 3c that the MIR spectra (20 $\mu m \leq \lambda \leq$ 50 μm) are almost featureless. The little spike at $\sim$ 100 μm is an artificial feature which may be due to the instrumental resolution (see Fig. 5 of Hudgins et al. 1993). The total dust mass required to produce the observed thermal emission is $\approx 2.25 \times 10^{27}\, g$ with $\approx 5.67 \times 10^{22}\, g$ in $[r_{inner}, r_1]$, $\approx 6.12 \times 10^{25}\, g$ in $[r_1, r_2]$ and $\approx 2.19 \times 10^{27}\, g$ in $[r_2, r_{outer}]$. Table 1 summarizes the parameters for the dust and the resulting dust masses. It is interesting to note that the fraction of the dust mass within the inner 40 AU is only $\approx 2.5 \times 10^{-5}$ of that of the total disk. If we had assumed a constant size distribution for the whole disk, this would have been ≈ 0.23. This implies that the inner 40 AU of the disk has been highly cleared out. This depletion has been suggested to be caused by the perturbations of planets (Roques et al. 1994; Lazzaro et al. 1994). On the other hand, the presence of a large population of small particles in the inner disk also indicates that they must be continuously replenished by some kind of dust-rich bodies since these small particles survive for only a short time in the inner disk due to the Poynting-Robertson drag and radiation pressure effects (Backman & Paresce 1993; Artymowicz 1988). The only available complete FIR/millimeter laboratory data for the optical constants of ice are for hexagonal ice. They are temperature dependent with the spectral index of the imaginary part of the index refraction n ($m'' \propto \lambda^{-n}$) ranging from $\sim$ 0.6 to $\sim$ 1.0 (Warren 1984). Because of the lack of FIR/millimeter data for the optical constants of amorphous and crystalline ices, we have tried to fit the FIR/millimeter emission by varying the spectral index n of the imaginary part of the refractive index of ice $m''_{ice}(\lambda)$ ($\propto \lambda^{-n}$) as discussed in Sect. 2.1. The best fitting to the FIR/millimeter emission as plotted in Fig. 3 implies that $m''_{ice}(\lambda) \propto \lambda^{-0.5}$ at $\lambda > 100\, \mu m$. For comparison, we present in Fig. 4 the theoretical spectra predicted by three sets of optical constants for ices: $m''_{ice}(\lambda) \propto \lambda^{-0.0}$, $m''_{ice}(\lambda) \propto \lambda^{-0.5}$, and $m''_{ice}(\lambda) \propto \lambda^{-1.0}$, respectively (keeping all other parameters unaltered). Fig. 4 clearly shows that the optical constants of ices at FIR/millimeter significantly affect the FIR/millimeter spectral energy distribution. Note that the variation of n in $m''_{ice}(\lambda) \propto \lambda^{-n}$ has negligible influence on the 10 μm silicate band and the MIR emission. In the following modeling, unless otherwise stated, we adopt $n = 0.5$.

The above calculations are based on the amorphous silicate model. Although it provides a good match to the general shape and width of the silicate spectrum, it fails (as expected) to reproduce the fine structure at 11.2 μm which is character-

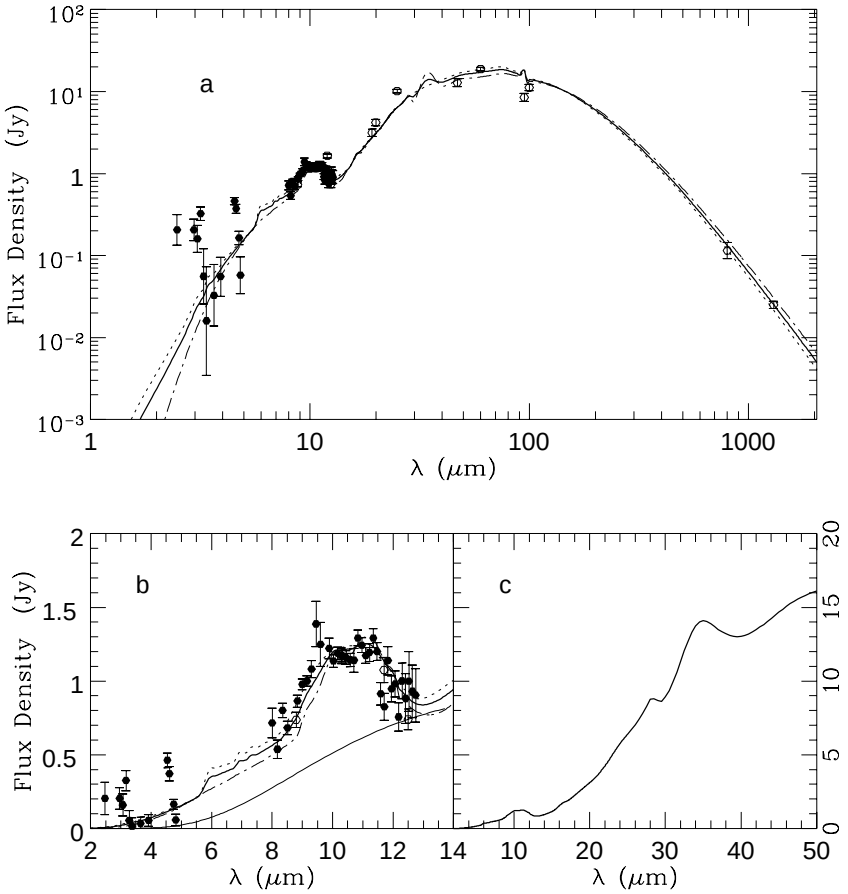

Fig. 9C. The spectral energy distribution predicted from a mixture of the amorphous silicate model (dotted line; same as Fig. 9A) and the crystalline silicate model (dot-dashed line; same as Fig. 9B) with an assumption of 30% crystalline silicates. **a** The overall spectra from the NIR to millimeter; **b** The 10 μm silicate feature; **c** The MIR emission bands.

istic of crystalline silicate. In the following we will first consider the pure crystalline silicate case – porous aggregates of crystalline silicates (with ice mantles in the outer region of the disk $r \in [r_2, r_{outer}]$ but no organic inner mantle). This represents the case in which not only are the grains heated in the internal region sufficient to create pure crystallinity but also to totally evaporate the organics. When such particles are in the outer region they may reaccrete H_2O but not the organics. The optical constants of crystalline silicate are based on the experimental results of Mukai & Koike (1990) and are extended to FUV and FIR/millimeter by us as discussed in Sect. 2.1. The effects of various crystalline silicate minerals on the 10 μm and MIR bands will be demonstrated in Sect. 5. The dust parameters are taken to be identical to those of the amorphous silicate model: $n(r) \propto r^{-2.7}$, r_{inner} = 1 AU, r_1 = 40 AU, r_2 = 100 AU, r_{outer} = 2200 AU; $n(m)$ same as in Fig. 2; P = 0.975; except M_{or}/M_{si} = 0 and M_{or}/M_{si+or} = 1.

Fig. 1b illustrates the grain temperatures as a function of the disk radius for the crystalline silicate model. From Fig. 1b it can be seen that the temperatures of crystalline silicate aggregates are significantly lower than those of amorphous silicate core-organic refractory mantle aggregates. This is due to the absence of organic refractory materials which are much more absorbing than silicates in the visual and near ultraviolet. The theoretical spectra are presented in Fig. 5. The overall spectral energy distribution is successfully fitted from NIR to FIR and millimeter,

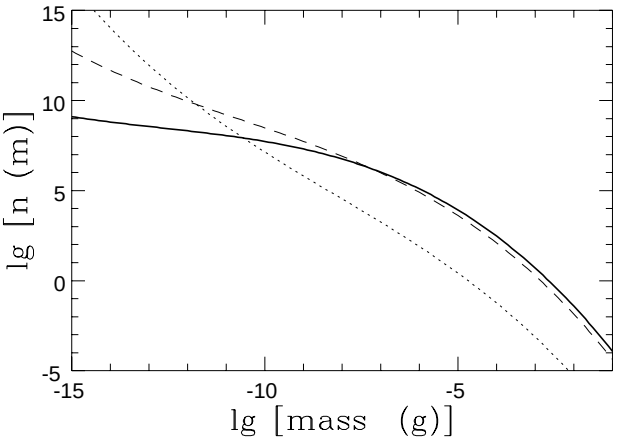

Fig. 9D. The mass (size) distributions of the dust grains which provide the spectral energy distributions shown in Fig. 9A and Fig. 9B.

except the silicate bands are too narrow (Fig. 5a). As illustrated in Fig. 5b, the model spectra show a distinct double-peak and provide an excellent match to the 11.2 μm emission and the red wavelength wing of the silicate band but there is a poor fit to the blue wavelength wing. Fig. 5c shows the predicted fine structures of the chosen silicate minerals in the mid-infrared (20 – 50 μm): 16.3, 18.6, 23.0, 28.0, 33.6 μm. Hopefully ISO will obtain high resolution spectroscopic data in this wavelength

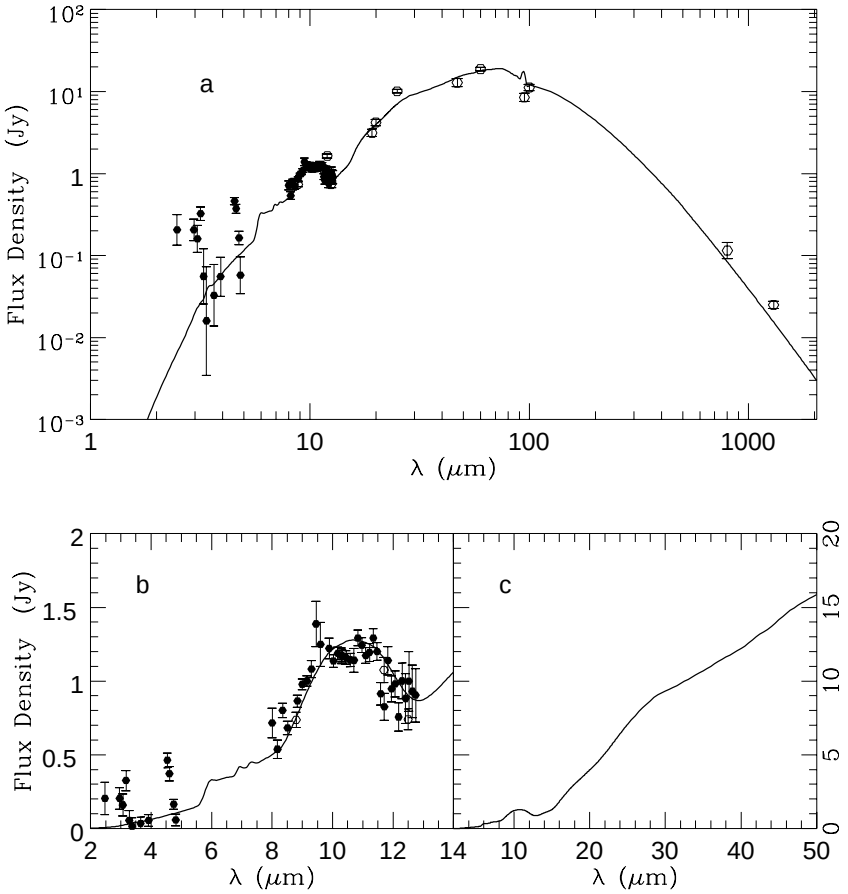

Fig. 10A. Same as Fig. 3 except the grain volume number density $n(r)$ goes as $\propto r^{-1.8}, r \in [r_{inner}, r_1]$; $\propto r^{-2.7}, r \in [r_1, r_2]$; and $\propto r^{-2.7}, r \in [r_2, r_{outer}]$ (see the text of Sect. 5.2). The grain mass distributions are shown in Fig. 10C.

region and place hard constraints on the silicate minerals in detail. This model results in a dust mass of $\approx 2.03 \times 10^{27}\,g$ with $\approx 2.40 \times 10^{22}\,g$ in $[r_{inner}, r_1]$, $\approx 5.60 \times 10^{25}\,g$ in $[r_1, r_2]$ and $\approx 1.97 \times 10^{27}\,g$ in $[r_2, r_{outer}]$ (see Table 1). The total amount of dust mass in the disk is close to that of the amorphous silicate model ($\approx 2.25 \times 10^{27}\,g$) while in the inner component ($[r_{inner}, r_1]$) the dust mass is only 42% of the amorphous silicate model. This is because the absorption cross section of pure crystalline silicate (at $\sim 10\,\mu m$) is about twice that of amorphous silicate core-organic refractory mantle particles.

Fig. 3 and Fig. 5 show that both the amorphous silicate model and the crystalline silicate model provide a satisfactory fit to the general spectra from the NIR to the FIR/millimeter. But neither of the two models is able to fully account for the silicate features in detail: the amorphous silicate model predicts a smooth feature which matches the observation quite well but fails to give the $11.2\,\mu m$ structure; while the crystalline silicate model provides a good match to the $11.2\,\mu m$ structure but results in a deficiency in the blue wavelength wing. This leads us to a model which consists of of two independent components: amorphous silicate core-organic refractory mantle aggregates and crystalline silicate aggregates as discussed in Sect. 2.1. For calculating the spectral energy distribution, we combine the results of the amorphous silicate model and the crystalline silicate model. The results of the combination of these two components are presented in Fig. 6A, Fig. 6B and Fig. 6C for several silicate mass ratios of the crystalline silicate model to the amorphous silicate model, $f = M_{crystalline}/M_{amorphous} = 0.20, 0.30, 0.40$, respectively. The fits to the observations are indeed improved. The best fitting model, $f = 0.30$, as illustrated in Fig. 6Bb, implies that $\sim$ 30% of the silicates in the disk have been converted into the crystalline phase. It is obvious that very large particles are cold and thus are not crystallized as efficiently as small particles. It is likely that the crystalline silicate aggregates distributed in the disk constitute only of those in the low mass part of the size distribution. Crystalline silicates are needed only to produce the $11.2\,\mu m$ feature and possibly the MIR bands with the FIR/millimeter emission dominated by the amorphous silicate aggregates. This will not affect the model fit of the MIR and FIR spectra since both the crystalline silicate model and the amorphous silicate model show a very similar behavior in the MIR and FIR. In other words the above derived mass fraction need only be valid in the *inner* components of the disk, so that only about 1% of the total silicates are required to be converted into the crystalline phase.

To check the accuracy of using simply the Planck function to represent the photospheric spectrum of β Pictoris, we have carried out a set of model calculations, adopting the fluxes of a Kurucz (1979) model with $T_{eff} = 8200$ K, log g = 4.25 (Crifo et al. 1997) and solar abundances. We found that the resulting grain temperatures are almost identical to those derived from the Planck function assumption (within 0.8%). Actually, the

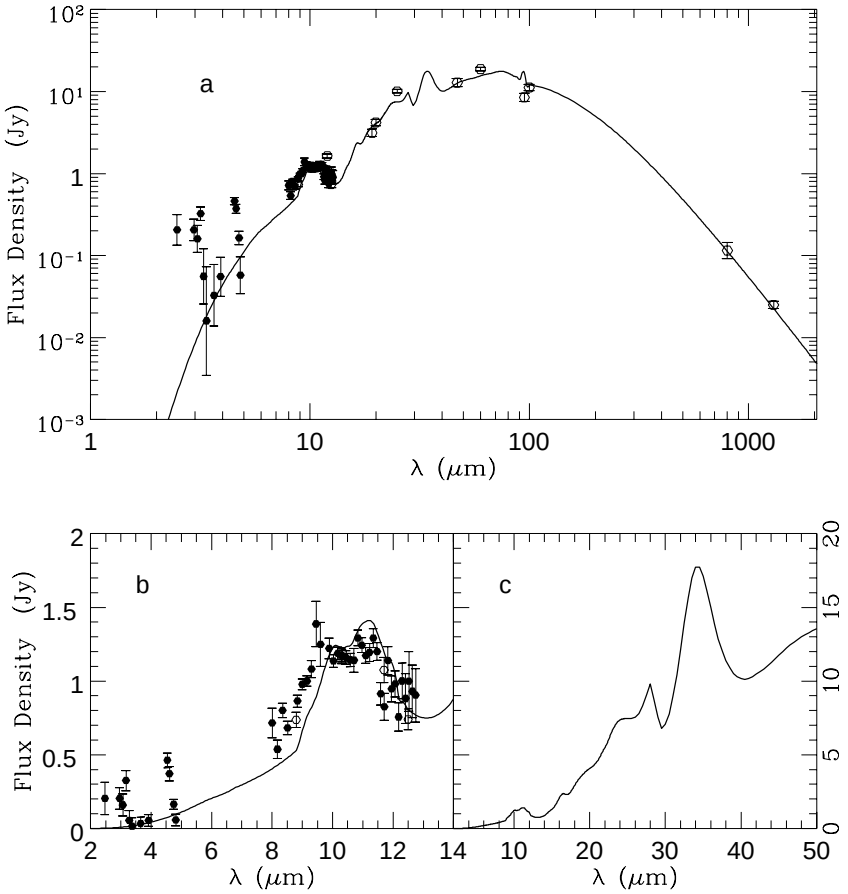

Fig. 10B. Same as Fig. 10A but for the crystalline silicate model.

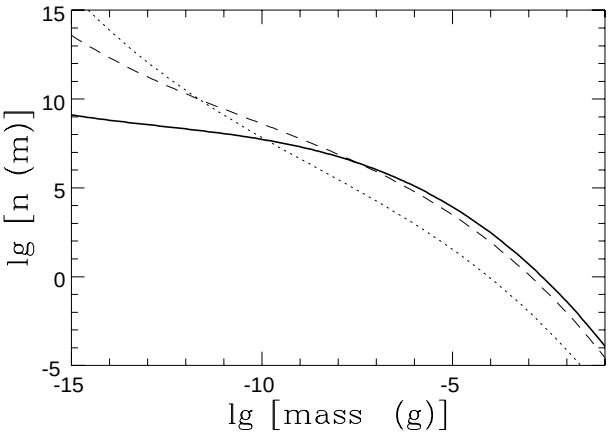

Fig. 10C. The mass (size) distributions of the dust grains which provide the spectral energy distributions shown in Fig. 10A and Fig. 10B.

Planck function closely resembles the Kurucz model spectrum down to $\lambda \geq 0.15\,\mu m$. A significant discrepancy occurs at $\lambda < 0.15\,\mu m$, where the Planck function is higher than the Kurucz model flux, but the heating contributed by photons in that range is negligible. Thus we conclude that, for the purpose of this work (with emphasis on the spectral energy distribution modeling), the Planck function assumption is sufficiently precise.

5. Discussion

In this section we shall first explore the model parameter space with emphasis on the porosity and the grain density distribution. We then investigate the possible influences of different crystalline silicate minerals on the $10\,\mu m$ and the MIR emission bands followed by a discussion of the gas species produced from the sublimation of the volatile components in the comet nucleus. After that a brief note on the possible astrophysical implications will be given.

5.1. The porosity

Starting with compact particles and adjusting the grain size distribution, it was easy to show that it is not possible to reproduce both the silicate feature and the MIR, FIR/millimeter emission at the same time: either the particles are too cold to give any silicate excess emission or there are too few cold particles to produce sufficient MIR, FIR/millimeter emission. We have initially tried to fit the observations using low porosity ($P < 0.975$) aggregates. We then considered fluffy particles with various porosities. For illustration, we present our model calculations for $P = 0.85$, $P = 0.90$ and $P = 0.95$ in Fig. 7, Fig. 8 and Fig. 9 respectively. Fig. 7A and Fig. 7B show the theoretical spectra predicted using $P = 0.85$ for the amorphous silicate model and the crystalline silicate model respectively. All the dust parameters derived for the $P = 0.975$ model (see Sect. 4)

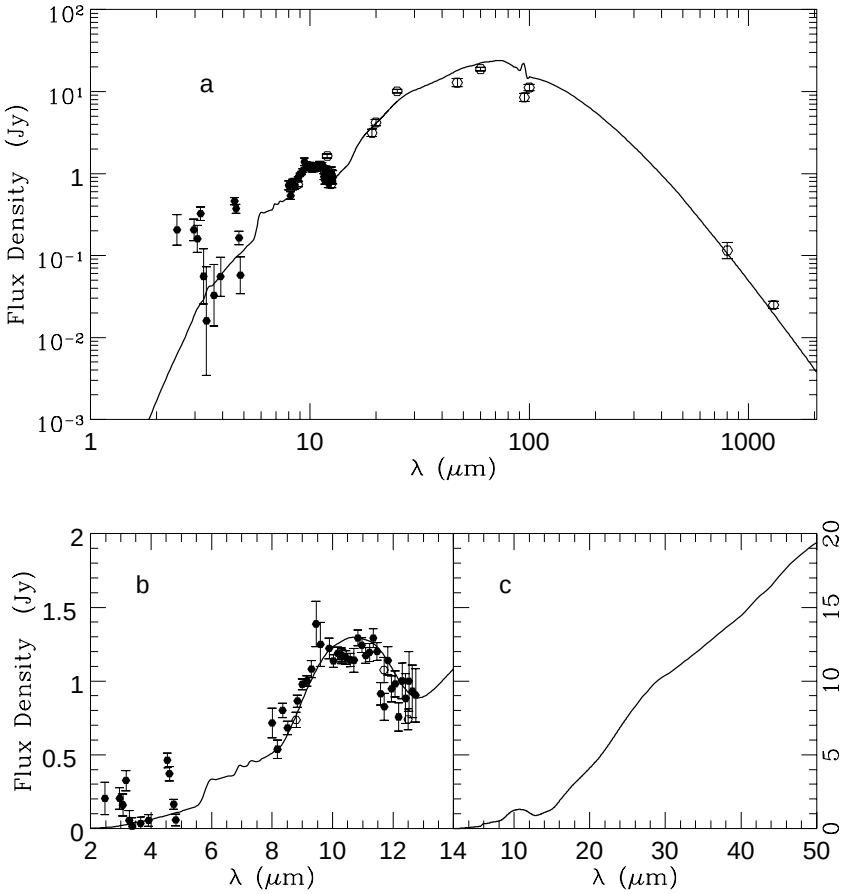

Fig. 11A. Same as Fig. 10A but for the grain volume number density falling off as $\propto r^{-1.8}, r \in [r_{inner}, r_1]$; $\propto r^{-1.8}, r \in [r_1, r_2]$; and $\propto r^{-2.7}, r \in [r_2, r_{outer}]$ (see the text of Sect. 5.2). The grain mass distributions are shown in Fig. 11C.

are unchanged except that the dust size distributions have been adjusted to provide the best fit to the observations. It can be seen from Fig. 7A and Fig. 7B that the P = 0.85 model gives a too shallow silicate feature and too little MIR emission. For the crystalline silicate model, the 11.2 μm feature shifts to a longer wavelength than observed. In Fig. 8A and Fig. 8B we present the model results for P = 0.90. The silicate feature is still too shallow compared to the observations. The model calculations are also deficient in the MIR. Thus both P = 0.85 and P = 0.90 aggregates are unacceptable.

It turns out that the P = 0.95 model provides a successful fit to both the overall spectral energy distribution and the silicate feature as good as or even a bit better than the P = 0.975 model. The model results for the amorphous silicate model, the crystalline silicate model, and the combination of both components are shown in Fig. 9A, Fig. 9B and Fig. 9C respectively. Fig. 9C implies that with $\sim$ 30% of the silicates in the crystalline phase the fine structures of the silicate emission can be reproduced. In this model all the dust parameters are identical to those of the P = 0.975 model (see Sect. 4) except, of course, for the porosity and the grain mass distributions which are plotted in Fig. 9D. As normalized, this is very similar to Fig. 2. The total dust mass required by this model, as listed in Table 1, is more than that of the P = 0.975 model, since for the higher porosity the particles are more absorbing and also emit more efficiently.

Based on Sect. 4 and the above discussion, one concludes that the dust grains in the disk of β Pictoris must be highly fluffy with a porosity around 0.95 or possibly as high as 0.975. It is noteworthy that *compact* dust particles with a size distribution of comet Halley dust also failed to produce an 11.2 μm structure (Mukai & Koike 1990).

5.2. The grain density distribution

As shown in Sect. 4, the observations are successfully reproduced by a model with a power law grain spatial density distribution $n(r) \propto r^{-2.7}$ along the entire disk ($r \in [r_{inner}, r_{outer}]$). We have also carried out calculations with different density distributions; i.e., different values for β ($n(r) \propto r^{-\beta}$). Although the model with a porosity P = 0.95 is as good as the one with P = 0.975 (see Sect. 5.1), we limit ourselves here for simplicity to the porosity P = 0.975. Following Artymowicz et al. (1989), we set β at 2.7 for the outer region of the disk ($r \in [r_2, r_{outer}]$). We found that it is possible to obtain a good match to the observation with other power laws by adjusting the grain mass distributions. In other words these two functions are coupled. Fig. 10A and Fig. 10B show that the observations are well fitted by a model with a grain density distribution of $\beta = 1.8, r \in [r_{inner}, r_1]$; $\beta = 2.7, r \in [r_1, r_2]$; and $\beta = 2.7, r \in [r_2, r_{outer}]$. Fig. 10C presents the corresponding grain mass distributions. A model with $\beta = 1.8, r \in [r_{inner}, r_1]$; $\beta = 1.8, r \in [r_1, r_2]$; and

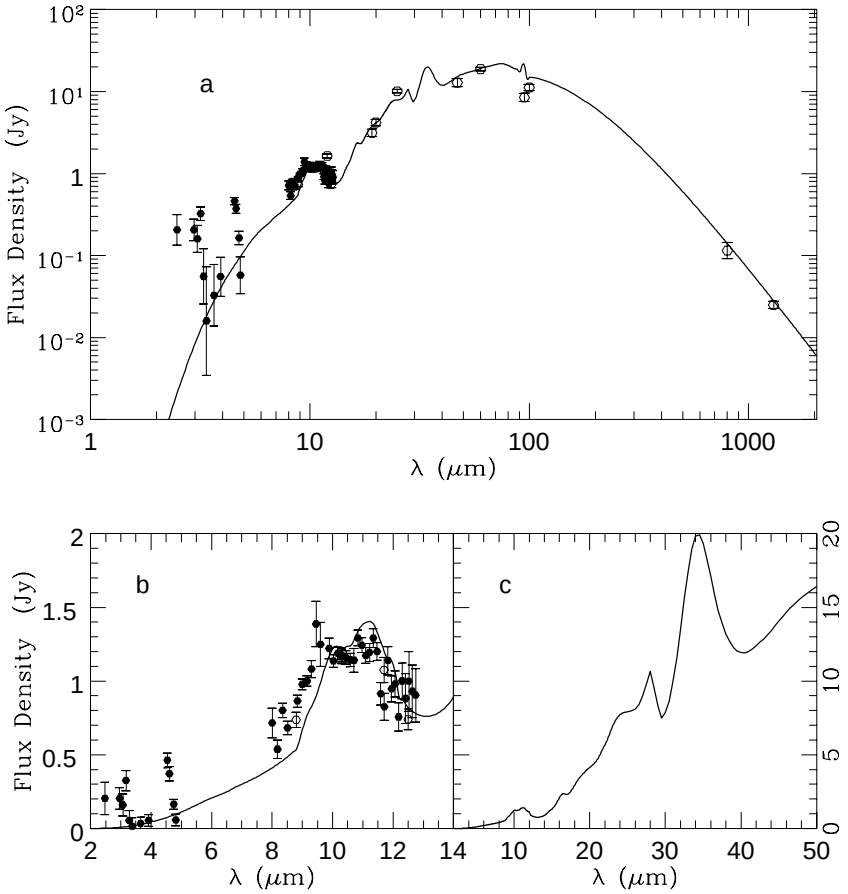

Fig. 11B. Same as Fig. 11A but for the crystalline silicate model.

$\beta = 2.7, r \in [r_2, r_{outer}]$ is also able to match the observation as illustrated in Fig. 11A and Fig. 11B if the grain mass distributions are as plotted in Fig. 11C. Note that another model, with $\beta = 2.0, r \in [r_{inner}, r_1]$; $\beta = 2.0, r \in [r_1, r_2]$; and $\beta = 2.7, r \in [r_2, r_{outer}]$ is also satisfactory (not shown here) with appropriate grain size distributions. The corresponding total dust masses required by these models are summarized in Table 1. We have to conclude that the grain density distribution is less well constrained than other parameters. However, the total dust mass (the combination of the grain density distribution together with the dust size distribution) is relatively well constrained ($\sim 2 \times 10^{27}$ g for all models, see Table 1). We also found that the grain density distribution in the inner component ($r \in [r_{inner}, r_1]$) cannot be too flat, otherwise there will not be enough hot particles to provide the the silicate emission; for example, for $\beta = 1.5$, the predicted silicate feature shifts to longer wavelengths and is also a bit lower than observed in the blue wavelength wing.

As shown by Lecavelier des Etangs et al. (1996), the model in terms of the evaporation of comet-like bodies is rather successful in accounting for the overall characteristics of the disk such as the asymmetry, the slope change of the scattered light profile, and the "wedge-like" shape, although they did not consider the details of the comet dust properties. From their work one can also see that the dust size distribution and the dust spatial distribution are coupled. Although we did not calculate the

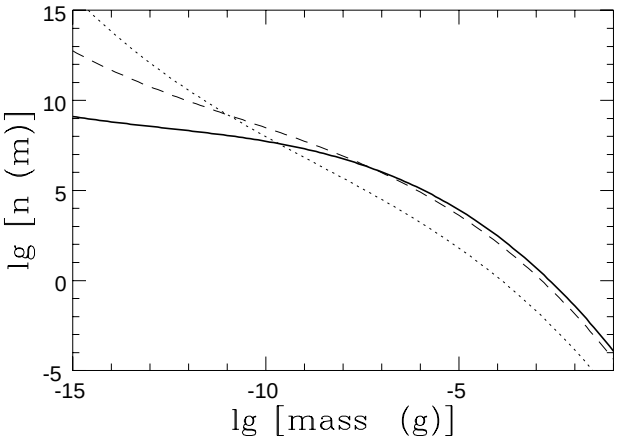

Fig. 11C. The mass (size) distributions of the dust grains which provide the spectral energy distributions shown in Fig. 11A and Fig. 11B.

scattered light distribution, we expect that our model would naturally predict the slope changes at $\sim$ 100 AU and at $\sim$ 40 AU due to the spatial variation of the dust size distribution (see Fig. 2, Fig. 9D, Fig. 10C and Fig. 11C).

Up to now, all discussions were made on the basis of the previous β Pictoris distance (D = 16.6 pc). When the new distance D$'$ ($\approx$ 19.28 pc) is adopted, all the previous geometrical dimensions ($r, r_{inner}, r_1, r_2, r_{outer}$) must be multiplied by a factor of

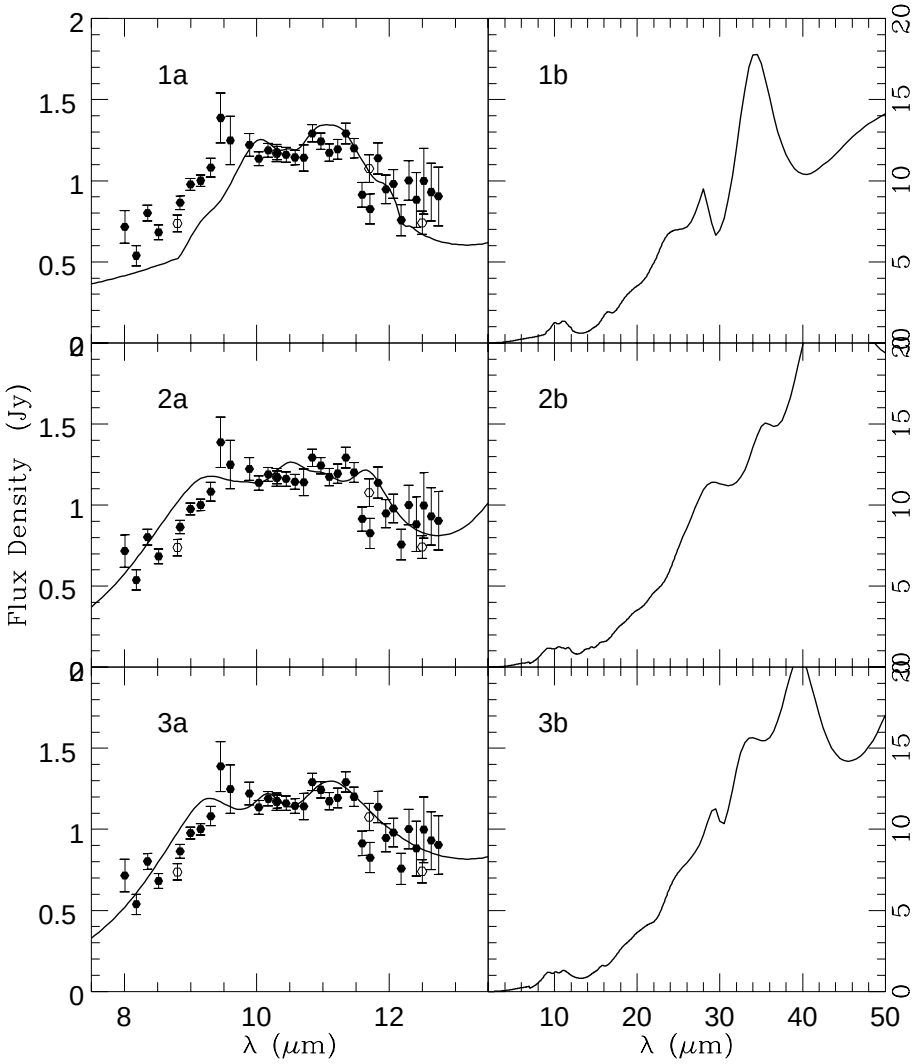

Fig. 12. The 10 μm silicate feature and the MIR emission band predicted from the crystalline silicate model in which the crystalline silicate mineral is: **1a**, **1b** crystalline olivine; **2a**, **2b** crystalline orthopyroxene; **3a**, **3b** crystalline clinopyroxene. All the other dust parameters are identical to those of Fig. 5.

$D^{'}/D$ (≈ 1.16) so that the dilution factor ω stays the same, and from Eq. 1 we can see that the radial ($r \times 1.16$) temperature distribution remains unchanged, thus the resulting spectral energy distribution and the silicate emission features do not change at all. However, from Eq. 2 we can see that the dust mass should be increased by a factor of $(D^{'}/D)^2$ ($\approx$ 35%). All the other quantities remain the same.

5.3. The crystalline silicate minerals

Olivine $Mg_{2x}Fe_{2(1-x)}SiO_4$ is a mixture of forsterite Mg_2SiO_4 and fayalite Fe_2SiO_4 with a mixing proportion x. Laboratory spectra of crystalline olivine with different forsterite content obtained by Koike et al. (1993) indicate that the infrared spectral features (both the strength and the peak wavelength) are slightly influenced by the magnesium/iron ratio. Generally, as the iron content increases, the spectral features become stronger and the peak positions shift to longer wavelengths. The optical constants of crystalline silicate adopted in this work are based on the experimental data of $(Mg_{0.9}Fe_{0.1})_2SiO_4$ (Mukai & Koike 1990). If the real crystalline silicate materials in the β Pictoris disk are richer in iron then one may expect that the 11.2 μm feature may be stronger than those predicted by the preceding models (e.g., see Fig. 7A, B, C) and it could improve our model fits to the observations. However, at this point we cannot say too much about the exact magnesium/iron ratio in the olivine since the spectral resolution of the observational data is not high enough, and there are no spectroscopic data in the MIR range which are also indicative of the magnesium/iron ratio.

So far the crystalline silicates have been confined to olivine. It is also of interest to consider crystalline pyroxene. We have tried to fit the observations using orthopyroxene and clinopyroxene. The optical constants of orthopyroxene and clinopyroxene are based on the latest experimental data of Koike & Suto (1996). The silicate feature and the MIR spectra provided by the best fitting models are plotted in Fig. 12. For comparison, those of the crystalline olivine model are also plotted in Fig. 12 (cf. Fig. 5; see Sect. 4). It can be seen from Fig. 12 that the orthopyroxene materials show no peak at 11.2 μm (Fig. 12-2a) and the model results in the blue wavelength wing being a bit too high relative to the observations. The clinopyroxene model provides a good

match to the overall silicate spectra (plus the 11.2 μm) except the predicted results are also a bit higher than the observations in the blue wavelength wing. The differences of the MIR spectra between the crystalline olivine, orthopyroxene and clinopyroxene are also apparent. The peaks are different both in position and in strength: for orthopyroxene the spectra peak at 28.5, 36.2, 44.0 μm (Fig. 12-2b); for clinopyroxene the peaks are at 29.5, 32.3, 33.7, 39.9 μm (Fig. 12-3b); and for olivine at 16.3, 18.6, 23.0, 28.0, 33.6 μm (Fig. 12-1b). Insofar as the 11.2 μm feature is concerned, the crystalline olivine is the most promising candidate. However, at this point we cannot rule out clinopyroxene as a possible candidate. High resolution spectroscopic observations in both the 10 μm region (including 11.2 μm) and the MIR should help to constrain the identification of the specific crystalline silicate minerals.

5.4. Comets as a source for the gas species in the β Pictoris disk

In the comet nucleus, the volatile components, accounting for about half of the total nucleus mass, lie in the ice mantles coated on the refractory components – the silicate core-organic refractory mantle dust particles (Greenberg 1998). As a comet approaches the central star in the β Pictoris disk, the volatiles sublimate due to the stellar insolation. If we assume a black-body temperature for the comet nucleus surface, $T_{BB}(r) \approx 458 \times r^{-1/2}$ K where r is the distance (in AU) of the comet from the central star, and adopt the sublimation temperatures listed in Crovisier (1997), we can qualitatively estimate that H_2O starts to sublimate at r $\simeq$ 9 AU, CH_3OH at r $\simeq$ 20 AU, NH_3 at r $\simeq$ 35 AU, CO_2 at r $\simeq$ 40 AU, H_2CO at r $\simeq$ 50 AU, CO at r $\simeq$ 360 AU. Note that these sublimation distances should not be considered as critical since the employed sublimation temperatures are for pure molecules, while the ice mantles as a mixture of various volatile molecules could behave in a much more complicated way (Crovisier 1997). In addition to the volatile molecules released directly from the nucleus, the evaporation of the organic refractory mantles may also contribute to the simple molecules such as CO, H_2CO, CN, C_2, C_3 etc. In comet Halley, the distributed CO, H_2CO molecules and the CN, C_2, C_3 jets are indeed of dust origin (Greenberg & Li 1997 and references therein). Since the organic mantles evaporate only in the innermost region (say, r $\leq$ 10 AU, see Fig. 1) where the dust grains are hot enough, due to the strong stellar UV radiation field, the molecules will photodissociate in a very short time scale ($<$ 1 month for H_2O, $<$ 1 year for CO). Even in the outer region, for example, at r = 100 AU, the photodissociation time scale is only about 6 years for H_2O and about 100 years for CO. Note that the H_2O molecules at such distances are not directly from the nucleus but from the sublimation of the icy dust grain mantles driven off by the molecules more volatile than H_2O. The CO gas molecules have been detected in the β Pictoris disk as a stable component both in UV (Vidal-Madjar et al. 1994; Jolly et al. 1998) and in submillimeter (Dent et al. 1995). Because of the short lifetime of CO molecules in the disk, they should also be continually replenished by comets as already noted in earlier works (Vidal-Madjar et al. 1994; Dent et al. 1995; Lecavelier des Etangs et al. 1996; Jolly et al. 1997).

If one really wants to push us to estimate the total CO mass predicted by our model, we can say that, the dust mass within the region r $\leq$ 100 AU indicates $\approx 6 \times 10^{23}$ g for CO, according to the arguments of Lecavelier des Etangs et al. (1996, see their Eq. 12; see also Jolly et al. 1997), in agreement with the HST-GHRS detection ($\approx 5 \times 10^{23}$ g; see Jolly et al. 1997).

5.5. The astrophysical implications

Amorphous silicates which exhibit broad, structureless 10 μm and 20 μm spectral features are ubiquitous in interstellar and circumstellar environments. Although crystalline silicates are not as common as amorphous silicates, observations do indicate the presence of crystalline silicates in various objects: comets (see Hanner et al. 1994 for a summary), Herbig Ae/Be stars (Waelkens et al. 1996), Vega-type stars (Knacke et al. 1993; Fajardo-Acosta 1996; Waelkens et al. 1996) and evolved oxygen-rich stars (Waters et al. 1996). Beta Pictoris may not be the only case which is characteristic of cometary particles. Indeed, the silicate feature of 51 Oph, which is also a Vega-type star, is very similar to that of β Pictoris and thus resembles those of comets (Fajardo-Acosta 1996). The fact that the gaseous CaII, CI and OI absorption lines of 51 Oph are similar to that of β Pictoris also implies the presence of infalling comet-like bodies (Lagrange et al. 1990; Grady et al. 1997). Recent ISO observations of the spectacular comet Hale-Bopp (Crovisier et al. 1997) have revealed a close similarity of the 6 – 45 μm crystalline silicate features of Hale-Bopp with those of HD 100546 (Waelkens et al. 1996), an intermediate star between Herbig Ae/Be stars and Vega-type stars in terms of age, while the ground-based observation made by Hayward & Hanner (1997) showed that the 8 – 13 μm spectrum of Hale-Bopp resembles those of other comets which exhibits both amorphous and crystalline silicate features. Similar to our model for β Pictoris, cometary objects have been proposed as a dust source for other systems (Harper et al. 1984; Matese et al. 1987; Grady et al. 1997). How universal this proposal is for the dusty disks of young stars and Vega-type stars awaits further study.

6. Conclusions

We have developed a model for the dust in the β Pictoris disk. The basic idea is that the dust in the disk plane is continually replenished by comets orbiting the star where the dust may be quickly swept out by radiation pressure or spiral onto the star as a result of Poynting-Robertson drag. We assume that the initial dust consists of fluffy aggregates of interstellar amorphous silicate core-organic refractory mantle tenth micron particles with an additional water dominated ice mantle in the outer region of the disk. When comets come close to the star, some dust aggregates are heated sufficiently to sublimate or evaporate not only the ice but the organic refractory mantle as well and may even crystallize the amorphous silicate so that there will be a new kind of dust – porous aggregates of crystalline silicates (no organic

mantle) in the disk. Exposed to the strong radiation pressure, both the initial aggregates of core-mantle dust and the new ones – aggregates of crystalline silicates – would be distributed over the entire disk plane. The inner boundary of the disk has been constrained to be $\sim$ 1 AU while the outer boundary extends to $>$ 2000 AU. The disk is divided into three regions in which the dust populations are responsible for the silicate emission, the mid-infrared emission, and the far infrared/millimeter emission respectively: $r \in [1, 40], r \in [40, 100], r \in [100, 2200]$. The presence of ice mantles only occurs in the outer region of the disk ($r \in [100, 2200]$). The grain size distribution is initially assumed to be like that observed for comet Halley dust while the evaporation and/or fragmentation of large particles in the inner components of the disk are assumed to lead to the enhancement of the distribution of small particles. The dust grains are very porous with a fluffiness or porosity around 0.95 or possibly as high as 0.975. Based on such a dust model, the predicted spectral energy distribution reproduces the observations (both the structured silicate feature and the continuum from near infrared to millimeter) very well. The total dust mass of the disk is estimated to be $\sim 2 \times 10^{27}$ g with only 10^{-5} – 10^{-4} of this in the inner component of the disk. This small fraction is hot enough to produce the silicate emission. If the newly determined β Pictoris distance 19.28 pc (rather than 16.6 pc) is adopted, with all the geometrical dimensions (r) multiplied by ≈ 1.16, our model results will not change at all, except the resulting dust masses should increase $\approx 35\%$. The crystalline silicate minerals have been discussed with a prediction of what may be possible to observe in the mid-infrared. The crystalline olivine may be the most promising candidate but the exact magnesium/iron ratio is not yet certain. Another silicate, clinopyroxene, cannot be ruled out at this point. The evaporation of the relatively more volatile ice mantles and the organic refractory mantles accounts for the gas species in the disk such as H_2O, CO, H_2CO etc.

Acknowledgements. We are grateful for the support by NASA grant NGR 33-018-148 and by a grant from the Netherlands Organization for Space Research (SRON). We thank Dr. S.B. Fajardo-Acosta and Dr. R.F. Knacke for providing us with the β Pictoris observational data, Dr. T. Kozasa for sending us the optical constants of crystalline olivine, Dr. C. Koike for providing us with the optical constants of crystalline orthopyroxene and clinopyroxene. We also thank Prof. T. Mukai, Dr. H. Okamoto, Dr. H. Kimura for their kind help in providing the optical constants of crystalline olivine. Useful suggestions from Prof. E.F. van Dishoeck, Dr. C. Dominik and Dr. W.A. Schutte are gratefully acknowledged. One of us (AL) wishes to thank Leiden University for an AIO fellowship and the World Laboratory for a scholarship. We thank the anonymous referee for helpful suggestions.

References

Aitken, D.K., Moore T.J.T., Roche, P.F., Smith, C.H. & Wright, C.M., 1993, MNRAS 265, L41
Artymowicz, P. 1988, ApJ 335, L79
Artymowicz, P., Burrows, C. & Paresce, F., 1989, ApJ 337, 494
Artymowicz, P., 1994, in: Circumstellar Dust Disks and Planet Formation, R. Ferlet & A. Vidal-Madjar (eds.), (Editions Frontieres: Gif sur Yvette), p.47
Aumann, H.H., et al., 1984, ApJ 278, L23
Backman, D.E., Gillett, F.C. & Witteborn F.C., 1992, ApJ 385, 680
Backman, D.E. & Paresce, F., 1993, in: Protostars and Planets III, E.H. Levy E.H., J.I. Lunine & M.S. Mathews (eds.), Tucson: University of Arizona Press, p.208
Beust, H., Lagrange-henri, A.M., Vidal-Madjar, A. & Ferlet, R., 1990, A&A 236, 202
Bohren, C.F. & Huffman, D.R., 1983, Absorption and Scattering of Light by Small Particles, Wiley, New York
Campins, H. & Ryan, E., 1989, ApJ 341, 1059
Chini, R., Krügel, E., Shustov, B., Tutukov, A. & Kreysa, E., 1991, A&A, 252, 220
Chyba, C.F., Owen, T.C. & Ip, W.-H., 1994, in: Hazards Due to Comets and Asteroids, T. Gehrels (ed.), Tucson: University of Arizona Press, p.9
Crifo, F., Vidal-Madjar, A., Lallement, R., Ferlet, R. & Gerbaldi, M., 1997, A&A 320, L29
Crovisier, J., Leech, K., et al., 1997, Science 275, 1904
Crovisier, J., 1997, in: Formation and Evolution of Solids in Space, J.M. Greenberg (ed.), Kluwer, in press
Day, K.L. & Donn, B., 1978, ApJ 222, L45
Dent, W.R.F., Greaves, J.S., Mannings, V., Coulson, I.M. & Walther, D.M., 1995, MNRAS 277, L25
Dominik, C., et al., 1997, in preparation
Draine, B.T. & Lee, H.M., 1984, ApJ 285, 89
Fajardo-Acosta, S.B., 1996, in: Physics, Chemistry and Dynamics of Interplanetary Dust, B.A.S. Gustafson & M.S. Hanner (eds.), p.507
Golimowski, D.A., Durrance, S.T. & Clampin, M., 1993, ApJ 411, L41
Grady, C.A., Sitko, M. L., Bjorkman, K.S., Perez, M.R., Lynch, D.K., Russell, R.W., Hanner, M.S., 1997, ApJ 483, 449
Greenberg, J.M., 1968, in: Stars and Stellar Systems, Vol. VII, B.M. Middlehurst & L.H. Aller (eds.), University of Chicago Press, p.221
Greenberg, J.M., 1978. in: Cosmic Dust, J.A.M. McDonnell (ed.), Wiley, p.187
Greenberg, J.M., 1982, in: Comets, L.L. Wilkening (ed.), University of Arizona Press, p.131
Greenberg, J.M. & Hage, J.I., 1990, ApJ 361, 260
Greenberg, J.M., Li, A., Mendoza-Gómez, C.X., Schutte, W.A., Gerakines, P.A. & de Groot, M., 1995, ApJ 455, L177
Greenberg, J.M. & Li, A., 1996, in: The Role of Dust in the Formation of Stars, H.U. Käufl & R. Siebenmorgen (eds.), Springer, p.161
Greenberg, J.M. & Li, A., 1997, in: Solar System Ice, B. Schmitt, C. de Bergh & M. Festou (eds.), Chapter 13, in press (a revised version has been accepted by A&A)
Greenberg, J.M., 1998, A&A 330, 375
Habing, H.J., Bouchet, P., Dominik, C., et al., 1996, A&A 315, L233
Hage, J.I. & Greenberg, J.M., 1990, ApJ 361, 251
Hanner, M.S., Tedesco, E., et al., 1985, Icarus 64, 11
Hanner, M.S., Tokunaga, A.T., Golisch, W.F., Grief, D.M. & Kaminski, C.D., 1987, A&A 187, 653
Hanner, M.S., Lynch, D.K. & Russell, R.W., 1994, ApJ 425, 274
Harper, D.A., Loewenstein, R.F. & Davidson, J.A., 1984, ApJ 285, 808
Harvey, P.M., Smith, B.J., DiFrancesco, J., Colome, C. & Low, F.J., 1996, ApJ 471, 973
Hayward, T.L. & Hanner, M.S., 1997, Science 275, 1907
Henning, Th. & Stognienko, R., 1996, A&A 311, 291
Hudgins, D.M., Sandford, S.A., Allamandola, L.J. & Tielens, A.G.G.M., 1993, ApJS 86, 713
Jolly, A., McPhate, J.B., Lecavelier, A., et al., 1998, A&A 329, 1028
Kalas, P. & Jewitt, D., 1995, AJ 110, 794
Kissel, J. & Krueger, F.R., 1987, Nature 326, 755

Knacke, R.F., Fajardo-Acosta, S.B., Telesco, C.M., Hackwell, J.A., Lynch, D.K. & Russell, R.W., 1993, ApJ 418, 440
Koike, C. & Tsuchiyama, A., 1992, MNRAS 255, 248
Koike, C., Shibai, H. & Tsuchiyama, A., 1993, MNRAS 264, 654
Koike, C. & Suto, H., 1996, in: Grain Formation Workshop, Vol. 18, p.67
Kouchi, A., Yamamoto, T., Kozasa, T., Kuroda, T. & Greenberg, J.M., 1994, A&A 290, 1009
Krügel, E. & Siebenmorgen, R., 1994, A&A 288, 929
Kurucz, R.L., 1979, ApJS 40, 1
Lagage, P.O. & Pantin, E., 1994, Nature 369, 628
Lagrange, A.M., Ferlet, R., Vidal-Madjar, A., 1987, A&A 173, 289
Lagrange, A.M., Ferlet, R., Vidal-Madjar, A., Beust, A., Gry, C. & Lallement, R., 1990, A&ASS 85, 1089
Lazzaro, D., Sicardy, B., Roques, F. & Greenberg, R., 1994, Icarus 108, 59
Lecavelier des Etangs, A., Perrin, G., Ferlet, R., et al., 1993, A&A 274, 877
Lecavelier des Etangs, A., Vidal-Madjar, A. & Ferlet, R., 1996, A&A 307, 542
Li, A. & Greenberg, J.M., 1997, A&A 323, 566
Little-Marenin, I.R. & Little, S.J., 1990, AJ 99, 1173
Matese, J.L., Whitmire, D.P., Lafleur, L.D., Reynolds, R.T. & Cassen, P.M., 1987, BAAS 19, 829
Maxwell-Garnett, J.C., 1904, Phil. Trans. R. Soc., London, 203A, 385
Mukai, T. & Koike, C., 1990, Icarus 87, 180
Mukai, T. & Mukai, S., 1984, Adv. Space Res. 4, 207
Pantin, E., Lagage, P.O. & Artymowicz, P., 1997, A&A 327, 1123
Paresce, F. & Burrows, C., 1987, ApJ 319, L23
Paresce, F., 1991, A&A 247, L25
Roques, F., Scholl, H., Sicardy, B. & Smith, B.A., 1994, Icarus 108, 37
Smith, B.A. & Terrile, 1984, Science 226, 1421
Smith, B.A. & Terrile, 1987, BAAS 19, 829
Telesco, C.M. & Knacke, R.F., 1991, ApJ 372, L29
Telesco, C.M., Becklin, E.E., Wolstencroft, R.D. & Decher, R., 1988, Nature 335, 51
Thomas, N. & Keller, H.U., 1989, A&A 213, 487
Tielens, A.G.G.M. & Allamandola, L.J., 1987, in: Interstellar Processes, D.J. Hollenbach & H.A. Thronson (eds.), Reidel, Dordrecht, p.397
Vaisberg, O., Smirnov, V. & Omelchenko, A., 1986, in: Proc. 20th ESLAB Symposium on the Exploration of Halley's Comet, ESA SP-250, II, p.17
Vidal-Madjar, A., Lagrange-Henri, A-M., Feldman, P.D., et al., 1994, A&A 290, 245
Waelkens, C., Waters, L.B.F.M., de Graauw, M.S., et al., 1996, A&A 315, L245
Warren, S.G., 1984, Applied Optics 23, 1206
Waters, L.B.F.M., Molster, F.J., de Jong, T., et al., 1996, A&A 315, L361
Weissman, P.R., 1984, Science, 224, 987
Zuckerman, B. & Becklin, E.E., 1993, ApJ 414, 793

This article was processed by the author using Springer-Verlag LaTeX A&A style file *L-AA* version 3.